

A Data-Driven Health Index for High-Voltage SF₆ Circuit Breakers

Master Thesis

Jippe van Dunné

A Data-Driven Health Index for High-Voltage SF₆ Circuit Breakers

by

Jippe van Dunné

to obtain the degree of Master of Science
at the Delft University of Technology,
to be defended on Thursday the 8th of June 2023, at 11:00.

Student number: 4573137
Faculty: EEMCS
Master program: Electrical Engineering
Specialisation: Electrical Power Engineering
Project duration: September, 2022 - May, 2023
Thesis committee: Prof. ir. P.T.M. Vaessen
Dr. ir. M. Ghaffarian Niasar
Dr. S.H. Tindemans
Ir. A.G.A. Lathouwers

Cover: Siemens 3AV1 FG Blue 145 kV live tank circuit breaker [1]
Style: TU Delft Report Style, with modifications by Daan Zwaneveld

Abstract

High-voltage circuit breakers protect and control the electrical power grid, making their reliability of the essence. Robustly assessing the technical 'health' of every circuit breaker in operation is key for an optimal maintenance strategy and safety measures, but is traditionally not performed in a data-driven, statistical fashion. The goal is to design an indexation method for the health of the high-voltage SF₆ circuit breakers of TenneT TSO NL using its available (monitoring) data. This indexation is performed through modelling the hazard rate of major and minor component failures with the Cox proportional hazards model. Failure modes and their causes are investigated using large-scale surveys on historical failure data and covariates for the model are chosen accordingly. The hazard rate for minor failures is found to be increasing with the asset's operating voltage level, its average switching frequency, certain manufacturers, and its relative SF₆ leakage rate, of which the last relation has not been modelled before to our knowledge. Using the model output, the circuit breakers' probabilities of future failure are estimated, shown to have some predictive power, and incorporated into a color-coded scoring system. Using this quantitative measure of their condition, the TSO should be able to better manage its asset portfolio and risks. However, data quality, especially for major failures, is found to be low and poses a limitation, as well as a possibility for future research.

Preface

Voor jou ligt zowel de bekroning als het einde van mijn studententijd. Ik ben heel dankbaar en tevreden voor de afgelopen 7 jaar, en de trots waarmee ik dit afsluit is daarom bitterzoet. Zowel in de studie als alles er om heen ben ik vrij geweest om mijn hart te volgen, en de dingen te doen die ik leuk vind. Ik heb veel geleerd en veel gelachen, en kan met zekerheid stellen dat ik deze tijd enorm ga missen.

De studie elektrotechniek heeft mij mateloos gefascineerd, en dat doet het nog steeds. Het elektr(on)ische domein is zo ongrijpbaar en abstract, maar ook zo wijdverbreid en onmisbaar, dat ik er soms deemoedig van word. Echter vind ik juist het mooiste aan studeren: de waardering die het je geeft, voor de dingen die anderszins gegeven lijken. De systemen overal om ons heen zijn door niemand allemaal te bevatten, en vormen hiermee een oneindige bron van verwondering voor mij.

Tegelijk ben ik net zo overdonderd door het sociale domein, en alle leuke mensen die ik in deze tijd heb ontmoet. Voordat ik mijn tijd hier definitief afsluit, wil ik graag deze gelegenheid aangrijpen om een aantal mensen te bedanken voor hun ondersteuning, gezelligheid, intellect en liefde: degenen die mijn studie zowel mogelijk als de moeite waard maakten.

- Mijn ouders, voor onnoemelijk veel; wie kan ooit zijn ouders voldoende bedanken?
- Mijn familie, en het geluk wat ik heb om in zo'n hartelijk gezelschap geboren te zijn.
- Eleiza, voor haar geduldig luisterende oor en oprechte interesse.
- Al mijn vrienden van de studie, en bij naam genoemd Sebas, Jurgen en Owen: wij hebben elkaar er lachend doorheen gesleept.
- Mijn bandgenoten, want muziek maken met vrienden vind ik het leukste wat er is. Jullie vormen mijn wekelijkse creatieve uitlaatklep.
- Mijn club met gezellige idioten, voor een hoop vertier en vriendschap.
- De VDK, voor hun grote regelmaat en lekkere eten.
- Mijn ploeggenoten bij Laga, waar ik alweer een tijdje weg ben, maar een groot deel heeft uitgemaakt van mijn studententijd. Roeien was niet de sport voor ons, en dat bond ons.
- Al mijn vrienden van de ETV, die het leven op de faculteit enorm verbreedden, en waar ik zoveel leuke dingen heb mogen helpen organiseren.
- Mijn bestuursgenoten bij het Sterkstroombispuut (SSD), met wie ik een jaar lang allerlei toffe excursies op touw heb mogen zetten voor onze mede-studenten.
- Mijn scriptie-begeleider André, voor onze gezellige wekelijkse afspraak, maar ook Mohamed, Simon en Peter, die ook in het proces van grote hulp zijn geweest.

Nu is het tijd voor de volgende stap, met een nieuw begin. Ik ben benieuwd en enthousiast over hoe de komende jaren zich zullen ontploegen!

*Jippe van Dunné
Delft, May 2023*

Contents

Abstract	i
Preface	ii
Nomenclature	v
1 Introduction	1
1.1 The Problem	1
1.2 Existing Methods	2
1.3 Scope of the Research	2
1.4 Main Results and Thesis Outline	3
2 Circuit Breaker Failure Analysis	4
2.1 Major Failures	4
2.1.1 The Distribution and Rate of Major Failure Modes	5
2.2 Minor Failures	6
2.2.1 The Distribution of Minor Failure Modes	6
2.3 Failure Mode Causes	7
2.4 Summary	8
3 Data Analysis and Transformation	9
3.1 Age	10
3.2 Manufacturer	10
3.3 Voltage Level	11
3.4 Relative SF ₆ Leakage Rate	11
3.5 Switching Frequency	12
3.6 Maintenance Intensity	12
3.7 Temperature and Relative Humidity	13
3.8 Time to Failure	14
3.9 Summary	15
4 Model and Estimation	16
4.1 The Cox Proportional Hazards Model	16
4.1.1 Why This Model?	17
4.1.2 Proportionality Assumption	17
4.1.3 Time to Failure Interpretation	17
4.2 Model Estimation Method	17
4.2.1 Coefficient Vector β	18
4.2.2 Baseline Hazard Rate λ_0	19
4.3 Proportionality Assessment	20
4.3.1 Visual Inspection	20
4.3.2 Time Since Last Failure	21
4.3.3 Manufacturer	22
4.3.4 Voltage Level	23
4.3.5 Relative SF ₆ Leakage Rate	24
4.3.6 Switching Frequency	24
4.3.7 Periodic Maintenance Intensity	25
4.3.8 Temperature	26
4.3.9 Relative Humidity	27
4.4 Regression Analysis	27
4.4.1 Correlation Assessment	27
4.4.2 Coefficient Estimates	28

4.5	Summary	30
5	Results	31
5.1	Estimated Model	31
5.1.1	Coefficient Vector β	31
5.1.2	Baseline Hazard Rate λ_0	32
5.2	Distribution of Estimated Failure Probabilities	33
5.3	Assessment of Predictive Power	34
5.3.1	Bifurcation of Probability Distribution into Failed and Non-Failed	34
5.3.2	Predictive Classification	35
5.4	Conversion to Color-Coded Score	36
5.5	Summary	37
6	Conclusion	38
6.1	Recommendations for Future Research	39
6.2	Recommendations for TenneT TSO NL	39
	References	40
A	Derivations	43
A.1	Derivation of Relation Between Survivor Function and Hazard Rate	43
A.2	Derivation of the MLE of α_i	44
B	Covariate Correlation Coefficients	46
C	Out-of-Sample Model	47

Nomenclature

Abbreviations

Abbreviation	Definition
ACM	Authority for Consumers and Markets, Dutch: <i>Autoriteit Consument & Markt</i>
AIS	Air-insulated switchgear
BRP	Bay Replacement Program
CB	Circuit breaker
CBM	Condition-based maintenance
CIGRE	International Council on Large Electric Systems, French: <i>Conseil International des Grands Réseaux Électriques</i>
Cox PHM	Cox proportional hazards model
DSO	Distribution system operator
FMECA	Failure Mode Effect & Criticality Analysis
GE	General Electric, a company
GIS	Gas-insulated switchgear
IEC	International Electrotechnical Commission
IED	Intelligent electronic device, an integrated microprocessor-based controller of power system equipment
ENTSO-E	European Network of Transmission System Operators for Electricity
HI	Health index
KNMI	Royal Dutch Meteorological Institute, Dutch: <i>Koninklijk Nederlands Meteorologisch Instituut</i>
NERC	North American Electric Reliability Corporation
SF ₆	Sulfur hexafluoride, an insulation medium
TBM	Time-based maintenance
TSO	Transmission system operator

Symbols

Symbol	Definition	Unit
F	Survivor function	none
F_0	Baseline survivor function	none
\hat{F}_0	Estimate of baseline survivor function	none
R_j	The set of labels associated with the CBs at risk, i.e. that have not failed or been censored at time t_j^-	N/A
T	Failure time	year
x	Covariate vector	N/A
β	Coefficient vector	N/A
$\hat{\beta}$	Estimate of coefficient vector	N/A
Λ	Cumulative hazard	none
Λ_0	Cumulative baseline hazard	none
$\hat{\Lambda}_0$	Estimate of cumulative baseline hazard	none
λ	Hazard rate	[1/year]
λ_0	Baseline hazard rate	[1/year]

1

Introduction

The electrical power grid is an essential part of the modern world. We depend on it for communication, health care, transportation, heating, entertainment and industry, among others. For this reason, maintenance of the electricity grid is of the utmost importance.

The Bay Replacement Program (BRP) is a large undertaking of TenneT TSO NL to this extent. Its goal is to replace 140 electrical substations in 10 years, most of which were constructed in the sixties and seventies of the previous century. Since many of the contained assets have a designated lifetime of forty to fifty years, their replacement is due. Furthermore, the stations' capacity typically needs to be increased due to the energy transition. For this large replacement wave, TenneT TSO NL is implementing a standardized and modular design for the bays of the substations including digitized protection and control, unlocking new inspection techniques. The goal of this is quick replacement of entire bays and a standardized maintenance strategy.

For an optimized maintenance strategy, knowledge of the technical condition of every component in every substation is required. This condition is referred to as *health*. The goal of this is to anticipate degradation or failure. At designated end-of-life however, it turns out that many components are still in a relatively healthy condition, contrary to what their time-based maintenance (TBM) schedule suggests. For this reason, TenneT TSO NL has decided to switch to condition-based maintenance (CBM). The health index (HI) is the means to this end: it incorporates data about the asset, such as its operating conditions, into a mathematical formulation. The output is a metric for its estimated probability of failure. Thereby, it provides insight into the states of individual assets in a population, and can discern between components with good and poor health.

There are three main motivations for a well-functioning health index: financial savings, security of supply and, most importantly, safety of people. Avoiding unnecessary maintenance saves money, whereas expedited or clustered maintenance can prevent more costly repairs or replacement. Furthermore, with increased insight in the health and thus probability of failure of the components, the security of supply is improved. Lastly, the avoidance of any unnecessary operations on high-voltage components decreases the associated risk of human life, the gravity of which cannot be overstated.

1.1. The Problem

Traditional health index models are based on age. However, failures are hard to predict based on solely this variable, as the rate at which component failures occur, i.e. the *hazard rate*, is approximately constant over time during maintained operation [2]. This difficulty is caused by the fact that components can fail in a multitude of ways, whereas the probability of failure(s) is estimated jointly. For this reason, more data is introduced into the model, to account for previously unforeseen failures.

The problem is the incorporation of this data for modelling the hazard rate. Not all failure modes can be anticipated, and different failure modes can be predicted at different horizons. Furthermore, not all desired variables are observable while the device is in operation and not all the observable data is actually monitored. On top of that, conditions that are monitored are usually sampled seldomly, through scheduled inspection procedures. Lastly, as these inspections are carried out by humans, it is not uncommon for reports to be riddled with (notation) errors.

All the aforementioned factors complicate the construction of a sound HI, but the advancing rollout of the IEC61850 protocol will remove some of these hurdles. This communication protocol for intelligent electronic devices in electrical substations introduces a myriad of sensors into the grid and its components to monitor various conditions continually. Through a glass-fiber network, these sensors are connected to the control center of the grid and their information is available almost instantly to the operators. This increases the amount of observed conditions, increases their observation frequency and removes human error from the reporting process. All these benefits percolate to a better grasp on the technical health of TenneT TSO NL's assets. In the BRP, this new protocol is implemented, creating the need for a HI that, in the future, can easily incorporate the added information.

1.2. Existing Methods

The existing health assessment methods can roughly be split into two categories: expert knowledge-based and data-driven models. The advantage of the former is that much qualitative knowledge is readily available at utility companies, whereas the quantitative data required for the latter are often lacking. However, the latter typically outputs a failure rate or related metric, whereas the former merely provides a (color-coded) score.

To the expert knowledge-based class belongs an overarching publication by CIGRE [3], which describes how to use failure data to perform a Failure Mode Effect & Criticality Analysis (FMECA). This process specifies condition indicators for every failure mode and lays out a five-level scoring system based on these indicators. It provides a heuristic and robust method to order diverse components based on weighted condition indicators, but does not assess the actual failure rate. Similar to this method are: the current TenneT HI [4] that uses a smoothed maximum function to concatenate scores based on age, previous failures and condition indicators; Ofgem's Common Network Asset Indices Methodology [5], a standardized asset indexation method for British DSOs; and various commercially available HI models, such as those of [6]–[10], of which a comprehensive assessment has been performed in [11].

To the data-driven class belong more academic models. A general model proposed in [12] encapsulates virtual age models, scale models, as well as regression models and their combinations. All these models' principle is a baseline failure rate depending on component age with various condition-based modifiers. Virtual age alters the perceived age, scale directly multiplies the failure rate and regression scales the failure rate through covariates proportional to the hazard rate, such as in the Cox model [13]. A similar but more specific virtual age model is published in [14], which allows for time-dependent covariates. This is convenient as monitoring data is typically time-varying. Another interesting approach uses monitoring data in hyper-dimensional boxes as alarm-triggers and is proposed in [15]. Furthermore, extensive research into the application of the proportional hazards model to high-voltage equipment and quantitative assessments of significance of explanatory variables are presented in [16]. Last is the failure mode-based model proposed in [17], which combines the FMECA basis of the first class with distribution fitting to assess how monitoring data affects the rates of specific failure modes. The model compiles these rates into a general failure rate through distribution fitting. This is an elegant model, albeit that the added stage requires more parameters and is prone to overfitting and overidentification.

1.3. Scope of the Research

The high-level goal of this research is to design a data-driven HI for TenneT TSO NL's high-voltage components to unlock smarter maintenance strategies. The HI should be constructed with an eye on the future of condition monitoring, while being able to work with the currently available data. As no IEC61850 data is yet available, the underlying model should be robust towards lower quality data, as is the status quo.

The thesis goal is restricted to the application to circuit breakers (CBs), as they are considered among the most complex high-voltage components. Only live tank, spring-operated, high-voltage, SF₆ CBs installed onshore are considered¹ due to the standardization of the BRP and for the sake of a

¹Live tank CB's enclosure is at line potential (i.e. 'live'), whereas the dead tank CB's is at earth potential (i.e. 'dead'). Both CB types are air-insulated switchgear (AIS), being placed separately from other components in the field insulated by air. Gas-insulated switchgear (GIS) is placed in a metal enclosure filled with a gaseous insulating medium along with other high-voltage components. Spring-operated CBs are driven by a compressed spring, wherein the energy for switching is stored. Other operating mechanisms include hydraulic, pneumatic and magnetic drives. Lastly, sulfur hexafluoride (SF₆) is the extinguishing medium inside the CB; other media include oil, air, CO₂ and vacuum.

uniform data set. This is the dominant type of CB in The Netherlands, making up 82.5% of the onshore population, as most older types are deprecated [18].

The scope of the HI is limited to the probability of failures, not their impact, for the sake of simplicity and feasibility of the study. The goal of the research is reached through the answering of the following research question, with three sub-questions:

- **How can the health of a live tank, spring-operated, high-voltage, SF₆ circuit breaker installed onshore robustly be estimated using currently available monitoring data?**
 1. What is the distribution and rate of circuit breaker failure modes?
 2. What variables can be used for estimating the hazard rate of the circuit breaker?
 3. How can the estimated hazard rate be translated into a health index scoring system?

1.4. Main Results and Thesis Outline

In this thesis report, a new HI is presented consisting of four steps, which correspond to the four chapters of the thesis' body. Throughout the report, a distinction is made between major and minor CB failures in both modelling and interpretation. Reason for this dichotomy is that the failures are categorized differently in literature and at TenneT TSO, and exhibit different data qualities. Below, these four stages are outlined, with their corresponding main findings.

Analysis of the component's failure behaviour is the first step. In this chapter, the failure modes, their corresponding rates and the overall failure rate of the component are investigated using large-scale international surveys of CB failures by institutions such as CIGRE, ENTSO-E and NERC. The results suggest that explanatory power can mainly be found in conditions that can indicate wear and aging of the component, as well as information concerning design, manufacturing and installation.

Harvesting and transforming data from TenneT TSO NL's database is the second step. This database contains information on all 2767 unique CBs that have been operational after 2016 in The Netherlands, with corresponding nameplate data, work orders, operating voltage, installation year and location, average temperature and relative humidity in its area. Furthermore, estimates of the relative SF₆ leakage rate and average switching frequency are constructed, as these variables will become available with the implementation of IEC61850. The data acquired from TenneT TSO NL is typically of low quality and the application of robust transformations is required to create workable variables. Furthermore, the signal for major failure, i.e. the decommissioning of the asset, is highly censored due to designated end-of-life. Minor failures are better observed in the data set.

Selection and estimation of the model is the third step. Of the available methods for estimating component health, the Cox proportional hazards model (PHM) is chosen, as it is a flexible 'workhorse' model with a proven track-record that requires no distributional assumptions on the input data. The model estimates a collective aging process which is multiplied with an asset specific relative risk component, depending on e.g. its operating voltage and manufacturer. Covariates are analyzed and selected based on explanatory power to form two models: one for major and one for minor failures. The results show that for the analysis of major failures, very little predictive power is available in the covariates. For minor failures, the CBs manufactured by Siemens show the highest increased risk and those by GE the lowest. Furthermore, risk of minor failure increases with the degree at which the CB leaks SF₆, the voltage at which it operates and the average frequency it switches at.

Analysis of the model output and conversion to a color-coded score is the fourth and final step. The coefficient values of the estimated total model fall in line with those found in the previous chapter. The risk of major failure is found to be increasing with age, whereas of minor failure it is approximately constant. The distribution of out-of-sample predicted failure probabilities for 2022 seems reasonable. Furthermore, splitting the distribution across actual failures in 2022 results in two significantly different distributions, suggesting predictive power. However, the model is unable to effectively predict failures in a binary fashion. Predictability is found to be higher for minor failures than major failures, with F-scores of 19.4% and 12.0% respectively. A four-level, color-coded ranking, based on estimated failure probabilities in the next five years, is therefore based on the former. The resulting ranking classifies the components in shares of 7% – 7% – 27% – 58% for the four levels, ordered from worst to best.

2

Circuit Breaker Failure Analysis

In this chapter, we investigate the distribution and rates of failures modes of live tank, spring-operated, high-voltage SF₆ circuit breakers. The dominant major and minor failure modes are highlighted. For a brief introduction to high-voltage circuit breakers, we would like to refer the reader to the appendix titled 'Introduction to Circuit Breakers' in [17].

The Usage of Large-Scale Surveys

CB failures do not occur often, as they are mitigated at great cost because of the impact of failure. This makes studying historical failure data difficult, as few data are available. This is a typical problem for survival analysis, as has been formulated in the Resnikoff conundrum [19]. Furthermore, different modes of failure can occur, each with own causes, rate and impact.

To mitigate this conundrum, large-scale studies are required to make a sound assessment of their failure modes. CIGRE has performed three world-wide surveys which are used to analyze failure rates, modes and their distribution [20]–[22]. Furthermore, [23] and [24] have compared these studies to observe trends and changes in failure rates¹. The above data is compared with NERC's 2017 – 2021 report of its Misoperation Information Data Analysis System [25] and ENTSO-E's 2000 – 2009 report on grid disturbances and fault statistics from Northern Europe [26], to assess homogeneity. However, as CIGRE's survey is the most extensive, this will be treated as leading.

Where possible, data from these surveys are filtered for specific circuit breaker type in question. Where this was not possible, it is disclaimed in the text. This is an essential step in the construction of the health index, as it shows which failure modes are relevant, and which are not. Failure modes can be associated with specific (monitoring) variables, and therefore provide us with insight into which might be relevant for accurate failure rate modelling.

2.1. Major Failures

According to the IEC, a major failure is defined as '*a failure [...] which causes the cessation of one or more of its fundamental functions*' [27]. For the CB, these functions are those of an ideal switch: a perfect conductor when in closed position, and a perfect isolator when in open position. Furthermore, switching between these states should happen safely and swiftly.

When the CB fails to follow these criteria, a major failure occurs. Typically, this occurs when switching operations fail to be executed by the breaker, though other major failure modes such as electrical breakdown of the insulation medium in open position or support structure failure also occur.

The effects of a major CB failure can be very grave, as the role of the device is to protect electrical equipment from damage caused by overloading or a short circuit. It works by interrupting the flow of current to the location of the fault, thereby isolating it from the rest of the grid. When the breaker is unable to isolate, the fault continues and a larger area will be shut off by CBs in the region, leading to more service interruptions. Major failures are therefore to be avoided at all cost.

¹It should be noted that [23] did not properly follow the completeness constraint as required by [22, p. 21]. However, in this case, the difference only amounts to 2% of the population.

2.1.1. The Distribution and Rate of Major Failure Modes

CIGRE recognizes twenty-two different major failure modes in its most recent survey, of which only six are specific and have a share of larger than 1% in the distribution. Therefore, the smaller sixteen categories are gathered in 'other' and mostly consist of electrical breakdown modes across different poles in various positions. Furthermore, it includes closing without command. The distribution of the total 618 failures observed over 127,971 circuit breaker years is depicted in Table 2.1². This data considers live tank SF₆, but does not discern drive type. However, it is given that 64.6% of the CBs in the population is spring-operated.

The distribution of failures across failure modes roughly resembles that of the report from NERC [25]. However, as NERC covers the U.S.A. and Canada, the dominant enclosure type is dead tank. As also reported by CIGRE's survey, dead tank circuit breakers exhibit lower failure rate. This means that, although the ratio between failure modes is comparable, the overall failure rate is lower with about a factor 2. It should be noted however that these surveys used different reporting policies and both typically experience under-reporting, so these results likely cannot be used for any statistical inference.

Table 2.1: Failure mode distribution of 618 observed major failures over 127,971 circuit breaker years, from the third world wide survey conducted by CIGRE [22].

Major failure mode	Share [%]	Failure rate per 100 CB years
Does not close on command	28.2	0.136
Does not open on command	12.9	0.063
Opens without command	6.8	0.033
Fails to carry current	1.5	0.007
Locked in open or close position	29.6	0.143
Loss of mechanical integrity	9.5	0.046
Others	11.5	0.055
Total	100.0	0.483

As can be seen from Table 2.1, the dominant failure modes are 'Locked in open or close position' with 29.6% and 'Does not close on command' with 28.2% of major failures. At some distance follows 'Does not open on command'. The respective associated failure rates indicate that the two leading failure modes can be expected to occur once every 700 circuit breaker years, and once every 1600 CB years the third leading failure mode.

All of these failure modes are related to switching. However, a distinction should be made between 'Does not open/close on command' and 'Locked in open or close position', as the latter indicates an alarm has been triggered by the control system, not a failure to operate on command. This implies a different failure cause.

The overall major failure rate reported in the most recent CIGRE survey is equal to 0.483 major failures per 100 CB years. When comparing this to the report of [24] and [26], we find they are in close correspondence: [24] reports a major failure rate 0.48 major failures per 100 CB years, whereas [26] finds 0.521.

'Does not open/close on command'

CIGRE's third survey shows this failure mode to be typically associated with failing drive or control systems [22]. The operating mechanism consists of the kinematic chain, piping and fittings, energy storage and motors among others. However, it should be noted that hydraulic and pneumatic CBs jointly compose 35.0% of the dataset, of which the drive system is proven to be less reliable. This is further illustrated by the fact that spring-operated CBs make up 64.6% of the population, but only contribute to 43.0% of the failures.

Spring drives also exhibit failures though, and switching failure modes remain among the dominant modes for this CB type. Exact results for live tank spring-operated SF₆ CBs are not available, but circumstantial results suggest that the ratio between failure modes remains approximately the same,

²Some data from this CIGRE survey had to be redacted, as CIGRE requires completeness of every failure report: a failure card and a population card. Furthermore, some results are published with and some without that of a prevailing country (we suspect the U.S.A.), as its response otherwise dominates the results. Fortunately, this is dead tank dominated country, only containing 10 major failures of live tank circuit breaker, meaning the effect is less than 2%.

with a slightly increased share in 'Locked in open or close position'. The overall major failure rate for live tank spring-operated SF₆ CBs decreases thereby with a factor of approximately 2.5, yielding a failure rate of approximately 0.2 major failures per 100 circuit breaker years, i.e. a major failure occurs once every 500 years.

'Locked in open or close position'

This failure mode is typically caused by alarm signals from the control system [22]. This control system monitors the CB to determine whether or not it is safe to operate. The leading cause for this failure mode is a lack of SF₆ in the enclosure [23].

The CB type under consideration is filled with SF₆ at a pressure of approximately 7 bar. To monitor the density of the gas, a pressure guard is installed. This guard is a pressure (and often also temperature) gauge of the gas, to determine the present SF₆ mass. Aging and wear can cause small gaps to form between the gasket and the aluminium flange. Through these gaps, SF₆ can leak out. When the pressure (or, if the guard is temperature compensated, mass) falls below a certain level, an alarm is triggered. The goal of this alarm is to avoid switching actions, as the shortage of extinguishing medium means that safe switching cannot be guaranteed. As SF₆ douses the arc, a shortage thereof means that a connection possibly cannot be (re)opened.

2.2. Minor Failures

Turning back to the glossary of the IEC, a minor failure is defined as *any failure of a constructional element or a subassembly which does not cause a major failure of the switchgear and controlgear* [27]. For the CB, this implies any malfunction that does not immediately cessate one of its fundamental functions.

Most of the minor failure modes are associated with leakages or rating changes. Their impact is therefore lower, but they can often be seen as precursors to larger failures in the future. Leakages of hydraulic fluid or insulating gas for example do not necessarily degrade switching performance short-term, but can disable the system further down the road. These minor failures should therefore be treated not only as failures, but as 'warning' signals for further malfunctioning.

2.2.1. The Distribution of Minor Failure Modes

CIGRE discerns between eight different minor failure modes in [22], of which only six are specific. Here, that number has been reduced to four distinct minor failure modes, one of which is a catch-all for changes in functional characteristics. These changes in functional characteristics are gathered, because their content is not strictly specified, making inference from it hard. Together, they capture changes in ratings, such as mechanical friction and the capacity of the grading capacitor. Furthermore, CIGRE includes an 'Other' category, of which the content is also not disclosed.

CIGRE signals high under-reporting for minor failures and therefore does not report failure frequencies. Furthermore, the data do not differentiate between AIS (both live and dead tank) and GIS CBs. However, of the total 6,655 reported minor failures 5,276 (79%) belong to live tank CBs. Moreover, the data does not differentiate between drive types, as is visible from the 'Air or hydraulic oil leakage in operating mechanism', which does not apply to spring-operated CBs. This implies that the weight of the other minor failure modes is undervalued, and should be treated with more severity than suggested by the results of the survey. The total distribution of minor failures is given in Table 2.2.

The distribution of minor failures cannot be compared with either NERC or ENTSO-E data, as they do not report minor failures. However, in the analysis of [23], the distribution is ratified when taking causal relation between major and minor failures into account. For example, if many 'Small SF₆ leakages' are reported, many 'Locked in open or close positions' are expected, as one can lead to the other.

'Small SF₆ leakage'

The dominant minor failure mode 'Small SF₆ leakage', making up 35.6% of all SF₆ CBs under consideration of the third CIGRE survey [22]. This failure mode can be seen as a precursor to the major failure mode 'Locked in open or close position', as one of the likely triggers for the alarm is insufficient SF₆ pressure, aside from communication or gas monitoring sensor failures. [23] supports this hypothesis, stating that insulation medium leakages lead to the CB being unable to operate.

Table 2.2: Failure mode distribution of 6,655 observed minor failures over 281,090 circuit breaker years, from the third world wide survey conducted by CIGRE [22]. Due to high under-reporting, failures rates are not reported.

Minor failure mode	Share [%]
Air of hydraulic oil leakage in operating mechanism	20.3
Small SF ₆ leakage	35.6
Oil leakage of grading capacitors	1.0
Change in functional characteristics	28.5
Other	14.6
Total	100.0

The leaking of SF₆ into the environment is harmful, as it is a powerful greenhouse gas. Leakage rates typically increase over time, dignifying attention spent on modelling this failure mode. In 2015, the assets of TenneT TSO NL leaked 0.28 %/y of its total banked SF₆ mass, i.e. 1,106 kg/y [4].

The potential leakage of gas is monitored by a pressure guard, which alerts the system when the pressure falls below a safe level. As discussed in the subsection 'Locked in open or close position' above, wear of the gaskets and flanges can cause gaps, which lead to leakages.

'Change in functional characteristics'

The second most dominant failure mode is 'Change in functional characteristics', which can entail various rating changes. Changes in these various aspects of the mechanism can decrease switching performance, such as the simultaneity of the poles or the breakdown voltage of the insulation medium. It is difficult to pinpoint to what major failure mode exactly will lead, if conditions worsen. Furthermore, the cause of this failure mode is also hard to capture.

2.3. Failure Mode Causes

The survey of [22] includes a request for cause of the failure. The original survey includes 23 different causes, which here is compressed to five, as most account for a share smaller than 1% of the total.

Table 2.3: Failure cause distribution of 618 observed major failures over 127,971 circuit breaker years and 6,655 observed minor failures over 281,090 circuit breaker years, from the third world wide survey conducted by CIGRE [22].

Primary cause	Major failure share [%]	Minor failure share [%]
Pre-operative cause	19.9	13.5
Corrosion	4.4	12.3
Wear/Ageing	42.3	55.9
Other	16.9	4.2
Unknown	16.5	14.1
Total	100.0	100.0

The dominant failure cause for all failure modes, both minor and major, is 'Wear/Ageing'. This amounts to 42.3% of the major failures and 55.9% of the minor failures. 19.9% of the causes of the major and 13.5% of the causes of the minor failures stem from before operation. This entails design, engineering and manufacturing faults, as well as incorrect transportation and erection, or incorrect instructions thereto. It should furthermore be noted that 16.5% of the causes of major and 14.1% of the causes of minor failures are unknown, which leaves almost all the other causes to be of negligible size.

The above results suggest that a relation may exist between circuit breaker failure rates and their manufacturers, installers and service providers, as these all concern pre-operative conditions. Furthermore, 'Corrosion' can depend on environmental factors such as temperature, humidity and salinity. Lastly, 'Wear/Ageing' can, among others, depend on factors such as the amount of loading and the number of performed switching actions.

However, 'Does not open/close on command' is found to be proportional to the amount of switching operations, whereas 'Locked in open or close position' is inversely so. This implies that 'Wear/Ageing'

can affect the CB in different ways, depending on its use. [23] analyzed results from the three world-wide surveys on CBs and found similar results.

2.4. Summary

The analysis of the distribution and rates of the CB failure modes from the surveys and reports above suggest that statistical predictive power may be found in monitored variables for both the major and minor failures. Turning to the dominant failure causes, research interest is sparked in manufacturers, contractors, environmental conditions, leakage rates and switch counters, among others. In the next chapter, we discuss the available data, with their appropriate transformations for log-linearity in the hazard rates and robustness.

3

Data Analysis and Transformation

We have acquired data the TenneT TSO NL company asset register (Dutch: *bedrijfsmiddelen register*) concerning 2,757 live tank spring-operated SF₆ high-voltage circuit breakers placed onshore. Together, these assets span 55,134 circuit breaker years between 1972 and 2022. A snapshot of this asset register, together with TenneTs SF₆ deposition register and work orders register has been taken on November 8th 2022.

Using these registers, we have made a data set of all registered circuit breakers that were in service between 2016 and November 2022. The data between the different registers is linked based on the circuit breaker identification code, which is unique to the asset.

The registers contain large amounts of missing, erroneous and scrambled data. The features that, after cleaning, are considered for analysis are depicted in Table 3.1 and are discussed below. Furthermore, two definitions for failure are considered.

Table 3.1: The covariates considered for the model with their transformations, as well as the two failure definitions.

Covariate	Transformation
Age	Time since construction year
Manufacturer	Reduced 27 different to 3 overarching manufacturers
Voltage Level	In three categories: 110/150 kV, 220 kV and 380 kV
Relative SF ₆ Leakage Rate	Average mass-percentage lost per year
Switching Frequency	Average number of switching operations per year
Preventive Maintenance Intensity	Avg. number of preventive maintenance operations per year
Temperature	Yearly average using interpolated KNMI weather stations
Relative Humidity	Yearly average using interpolated KNMI weather stations
Time to Major Failure	Age at replacement
Time to Minor Failure	Mean time between corrective maintenance operations

A note on the future

Currently, TenneT TSO NL is rolling out continuous monitoring of high-voltage components in their bay replacement program [28]. This monitoring system is implemented through the IEC61850 protocol. Advantages of this online monitoring approach are a larger amount of available data which allows for easier and better analysis of the health of the component, less risk of human life as fewer in-person inspections are required and expected higher data quality, as most of the errors in the current data sets are human-made.

For the circuit breaker, the following data will (where applicable: continuously) be monitored under IEC61850 [29]:

- The waveform of the motor current, which provides an indication of mechanical resistance
- The switched current at every switching action, which relates to the energy dissipated in the CB

- Waveforms of the trip coil current, which shows the electrical actuation of the drive system.
- SF₆ density, twice a day, to measure possible leakages
- The total number of switching operations, to assess CB wear
- Simultaneity of the poles, both at closing and opening, which affects the power quality of the grid and indicates a degraded drive system
- Opening and closing time of the circuit breaker, which should be fast enough to minimize arcing
- Temperature outside the cabinet, which affects the dew point of SF₆ and rust formation
- Relative humidity outside the cabinet, which affects rust formation.
- Brand, type, software version, control settings of and error notifications from connected IEDs

Currently, this data is not available, though it is expected to be in the near future. However, (some of) the information contained in 'SF₆ pressure', 'Number of switching operations', 'Temperature outside the cabinet' and "Relative humidity outside the cabinet" is estimated using different data, albeit usually of inferior quality. The construction of these estimates is discussed in the following respective sections.

3.1. Age

From the circuit breakers' construction years in the company asset register, their ages are derived. Figure 3.1 shows the age distribution of the population. TenneT TSO NL handles a projected lifetime of forty years for circuit breakers and plans replacement after that. However, some assets reach a prolonged life, due to difficulty in outage planning, requiring N-1 under maintenance.

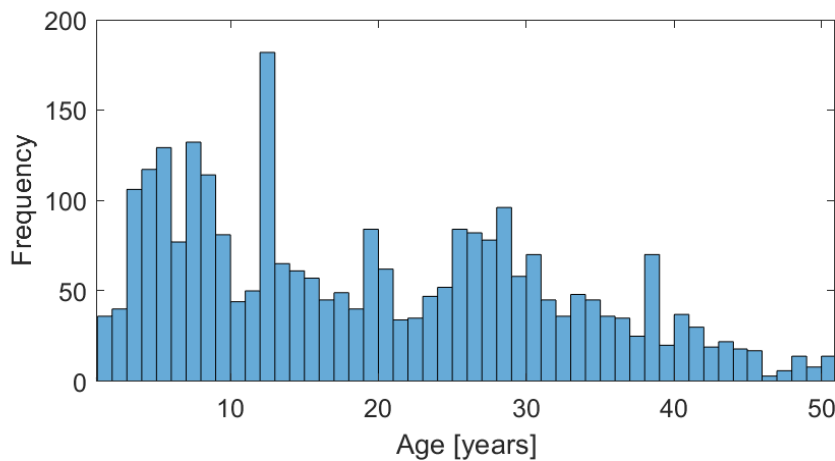


Figure 3.1: A histogram of the distribution of the ages of all the circuit breakers in the population.

3.2. Manufacturer

The initial amount of original manufacturers of 27 is reduced to 3 manufacturers: Siemens, General Electric (GE) and Hitachi. The reason for this reduction is robustness of the model and that these three companies currently own all others and therefore remain the only relevant manufacturers for future implementations.

The distribution of the manufacturers is shown on the left side in Figure 3.2 and to be relatively equal. This manufacturer parameter is modelled as two dummy variables, as shown in Table 3.2

Table 3.2: Coding of the two dummy variables for the reduced amount of manufacturers of the circuit breakers.

Manufacturer	Coding	
GE	1	0
Hitachi	0	1
Siemens	0	0

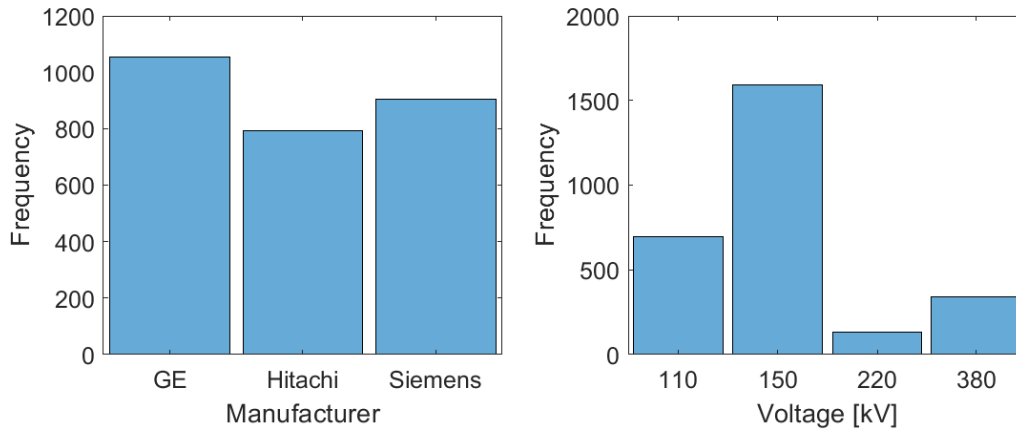


Figure 3.2: Histograms of the distribution of the manufacturers (left) and the operating voltage levels (right) of all the circuit breakers in the population.

3.3. Voltage Level

The distribution of voltage levels at which the circuit breakers are placed is depicted on the right side of Figure 3.2. TenneT TSO NL manages the 110 and 150 kV network since 2008, when the Law Independent Grid Operation (Dutch: *Wet Onafhankelijk Netbeheer*) was passed. The circuit breakers in these networks make up the lion's share of the total distribution.

Naturally, 110 and 150 kV circuit breakers are more predominant, as lower voltage networks are further down in the distribution hierarchy. It should be noted that the 'names' of the four voltage levels of the network are not always equal to the actual voltage residing on them. To increase the capacity of the network, the voltage may be increased if this stays within safety regulations.

The voltage levels are treated as categories for three reasons. First, the exact voltage of the network levels are not known and are susceptible to change. Second, the different levels involve different maintenance strategies (or histories thereof), further clouding the effect of the actual voltage. Last, categorized voltage levels have in the research of [30] been shown to have significant explanatory power.

In section 4.3, it will be shown that 110 and 150 kV CBs show similar risk exposure to this covariate, for which reason these are categorized together. The categories are coded with dummy variables as depicted in Table 3.3.

Table 3.3: Coding of the two dummy variables for the reduced amount of operating voltage levels of the circuit breakers.

Voltage level [kV]	Coding	
110/150	1	0
220	0	0
380	0	1

3.4. Relative SF₆ Leakage Rate

SF₆ leakages or pressure decreases are not recorded by service engineers. As SF₆ is a greenhouse gas however, its use is regulated and has to be reported to The Netherlands Authority for Consumers and Markets (ACM, Dutch: *Autoriteit Consument & Markt*)¹. Therefore, the deposited mass of SF₆ gas at maintenance and date has to be recorded for every filling. From these records, the leakage can be estimated.

Leakage rates are estimated over the entire lifespan of the circuit breaker, as the poor quality of these filling records did not lead to sensible estimates. For this reason, the relative leakage rate is

¹SF₆ is 22.800 times more potent than CO₂ and has an atmospheric lifetime of 3.200 years.

estimated:

$$\text{Relative SF}_6 \text{ leakage rate } [\%/y] = \frac{\text{Total mass of refilled SF}_6 \text{ [kg]}}{\text{Tank capacity [kg]} \cdot \text{Age [y]}} \cdot 100\% \quad (3.1)$$

Both the recording of the date and the amount of deposited gas per filling contain many erroneous data, leading to clearly incorrect parameter estimates. For this reason, both the mass and moment of the refill are smoothed by estimating the relative leakage rate over the complete lifetime of the circuit breaker.

The distribution of the 203 non-zero relative leakage rates are depicted in Figure 3.3. As can be seen, some circuit breakers leak exorbitant amounts of gas. The remaining 2,553 of the 2,757 circuit breakers have no records of refilling. This is inaccurate, as the work orders register shows many refilling events, of which no record exists in this SF₆ deposition log. However, this work order data is too noisy to be used.

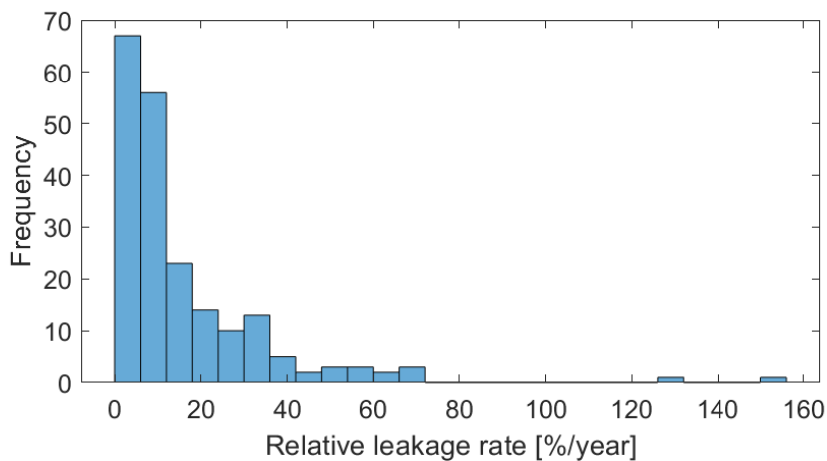


Figure 3.3: A histogram of the distribution of the estimated relative SF₆ leakages rates of all the registered leaking circuit breakers in the population.

3.5. Switching Frequency

High-voltage CBs feature a mechanical switch counter, which records the total amount of switching operations performed by the breaker. The position of this counter is recorded at inspection by TenneT TSO NL. As a significant part of failures can be attributed to mechanical wear, the amount of operations is important from a modelling perspective.

Using the time-stamped switch counter records, the average amount of switching operations per year for every circuit breaker is estimated. 899 of the 2,757 have registered recordings of their switch counter and the distribution of these averages is depicted in Figure 3.4, with a logarithmic frequency axis, to show both the frequent and infrequent counter readings.

As can be seen from the figure, most CBs do not switch often. The CBs that do switch frequently are typically connected to compensation devices, such as capacitor banks, as these are (dis)connected when they are required for reactive power compensation. These devices are typically switched at high currents, possibly introducing endogeneity for this unobserved covariate.

3.6. Maintenance Intensity

Work orders are registrations of service operations performed on the assets in the field. The work orders contain the identification code of the asset, the type of maintenance (either periodic or corrective), the type of service (e.g. repair, gas refill, inspection), the date, a description of the work performed and more.

TenneT TSO NL has granted access to 7,263 CB work orders between 1998 and 2022, of which 3,446 belong to the circuit breakers found in the company asset registry. The dating of the work orders

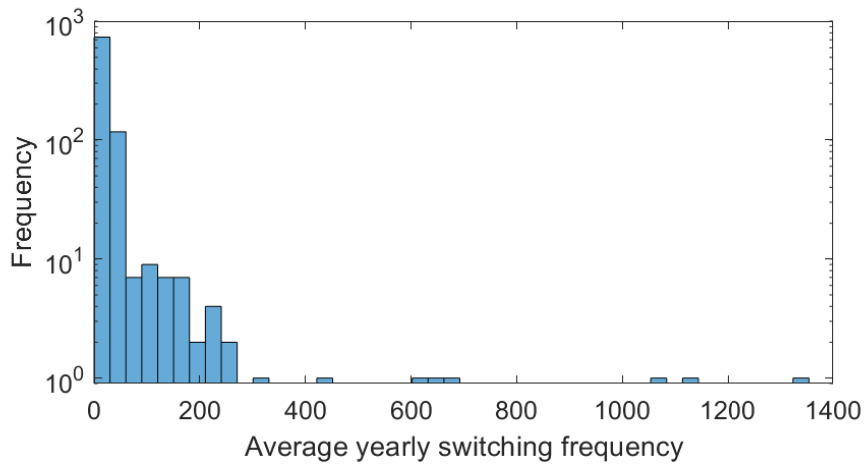


Figure 3.4: A histogram of the distribution of the average number of switching operations per year of the circuit breakers in the population. Note the logarithmic Y-axis.

is disregarded, as this is distorted. An exorbitant amount of work orders is either dated on October 1st 1998 or July 23rd 2004, making up 43.7% of the population. The average amount of service operations per year for each circuit breaker is used however, and a histogram of the non-zero results is depicted in Figure 3.5. 1,920 of the 2,757 circuit breakers have no records of past service.

For analysis, the work orders are split into periodic and corrective maintenance operations. The former is a scheduled service operation, while the latter is unplanned repair service. 527 circuit breakers in the population have experienced (registered) periodic maintenance, in comparison to 603 that have experienced (registered) corrective maintenance. As can be seen in Figure 3.5, the distributions of both are comparable, but their implications differ.

Periodic maintenance is expected to lower the hazard rate, as it could mitigate upcoming issues. Corrective maintenance in itself is essentially a failure, albeit a minor one. In this way, a high corrective maintenance intensity implies a high minor failure rate. For this reason, corrective maintenance is treated as a signal for minor failures, as will be discussed in section 3.8.

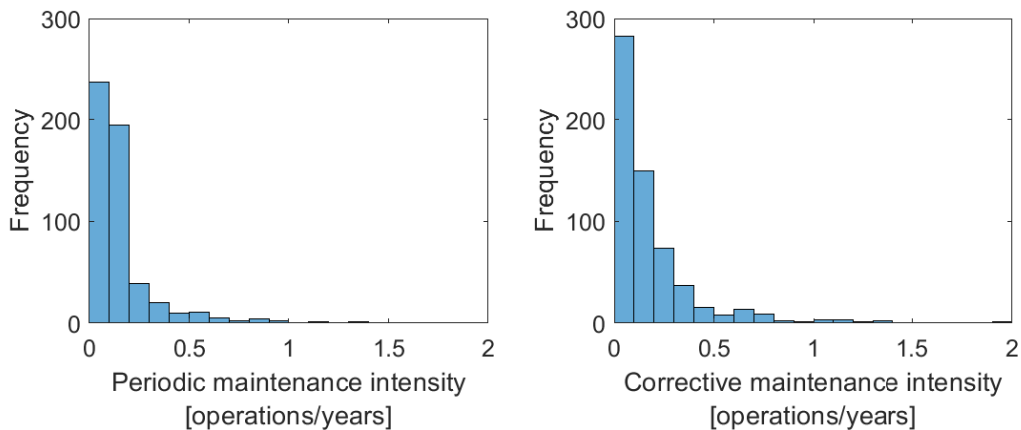


Figure 3.5: Histograms of the distributions of the non-zero work order intensities, both periodic (left) and corrective (right), of all the circuit breakers in the population.

3.7. Temperature and Relative Humidity

Year-averaged data of KNMI measurement locations are interpolated to the substation coordinates to get an estimate of the average temperature and relative humidity the circuit breakers are exposed to. An overview of the year-averages can be seen in Figure 3.6. This is a different approach from previous

research.

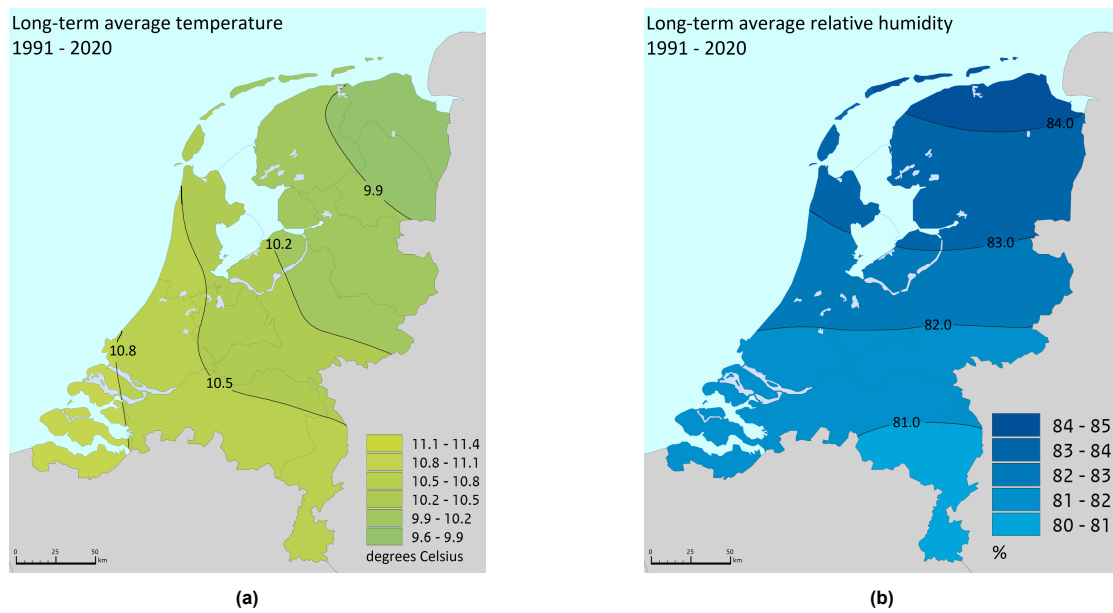


Figure 3.6: Long-term averages of the temperature (a) and relative humidity (b) in The Netherlands. Source: [31]

In the study of [30], the failure rate of the circuit breakers in Sweden are modelled using, amongst others, their geographical area. The installation locations are grouped in four regions using three dummy variables and a reference regions. Of these four regions, only one shows significantly different circuit breaker aging.

Regional divisions in The Netherlands are deemed inappropriate, as geographical differences in such a small country appear negligible in comparison². Furthermore, divisions into regions by dummy variables eliminate the explanatory power of the actual affecting quantities. Lastly, salinity measurements were also desired, but not available.

3.8. Time to Failure

Two signals for circuit breaker failure are considered: replacement of the circuit breaker and the performance of corrective maintenance. The resulting time to failure distributions are depicted in Figure 3.7. Typically, these events correspond to major and minor failures respectively, where the definition of major and minor failure are adapted from the IEC standard [27]. In short, major failures result in an immediate change of the operation of the grid, whereas minor failures do not.

Major failures are rare and replacement is often scheduled as planned end-of-life. No data register exists where major failures or unplanned replacements are recorded accurately. Therefore, even though this signal is distorted, it is the only option to model major failures. Furthermore, not all units are observed until failure, making them right-censored. Right-censoring is equal to 90.6% under this definition, as only 9.4% of the components (259 units) in the data set have been replaced.

Another approach is modelling the minor failures, as they occur more frequently and are registered more clearly. The corrective maintenance operations are considered as signal for minor failures. These are extracted from the work orders of section 3.6. The right-censoring in this case decreases to 78.1%, meaning 21.9% of the components (603 units) have experienced reported minor failures. The description and time-stamping of the performed maintenance typically lack and any further information on the failure is therefore deemed unusable. Note that, using this signal, one circuit breaker could experience multiple failures, whereas with the former it could not. Therefore, the time to failure is taken as the mean time between corrective maintenance. Here, the fact that the work orders are left-censored, as no registrations exist before 1998, is taken into account. The latter is the cause for the granularity

²Average temperature differences over the span of the country are around 1 °C, humidity differences around 4%, number of rainy days around 20 days and average wind speed differs from 2 to 4 Beaufort [31].

spikes at 24, 12 and 8 years, corresponding to circuit breakers older than 1998 that have experience 1, 2 and 3 minor failures respectively.

These two approaches lead to different interpretations of the failure rate of a circuit breaker. Using the time until decommissioning, the failure rate becomes the major failure rate, and similar for the mean time between corrective maintenance and minor failure rate. This is accounted for when analyzing the results.

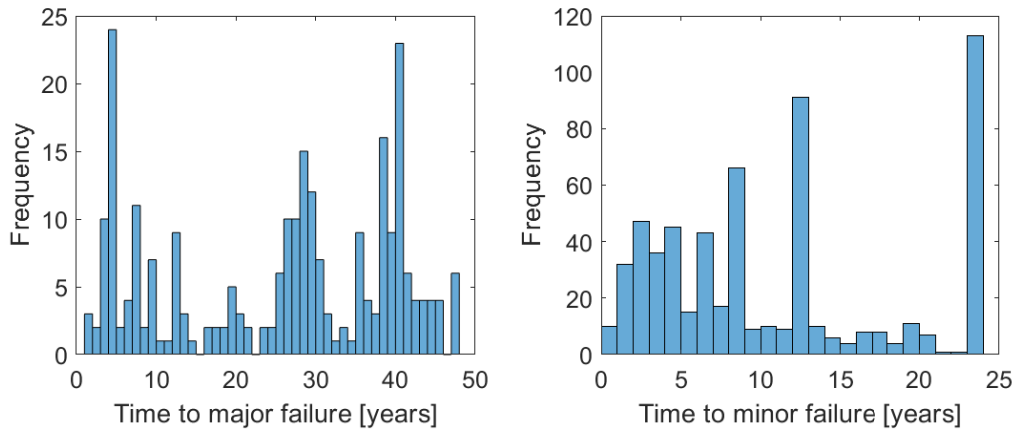


Figure 3.7: Histograms of the non-censored time to failure distributions of all the circuit breakers in the population. Left displays the age at major failure (decommissioning), whereas right displays the mean time between minor failures (corrective maintenance).

3.9. Summary

The harvested data are of mediocre quality, but after transformations robust enough to continue to modelling. We have gathered data on covariates deemed interesting in the previous chapter and include: the age of the asset, its (parent) manufacturer, the voltage level at which it operates, an estimate for its estimated SF_6 leakage rate, an estimate for its average switching frequency, the intensity at which it experiences preventive maintenance and an estimate for the average temperature and relative humidity of its environment. Last, we have gathered data for both major and minor failures, with respective right-censoring percentages of 90.6% and 78.1%.

4

Model and Estimation

In this chapter, we present the model chosen from the methods discussed in section 1.2, as well as the techniques used for its estimation. Furthermore, we analyze the available covariates shown in Table 3.1 for their explanatory power and significance, before a selection is made.

This selection process is conducted for both the major and minor failure approach to failure times, as discussed in section 3.8. First, we assess the proportionality assumption through visual, univariate inspection. Second, we investigate the significance of the explanatory power of the covariates by multiple regressions, for the composition of the final model.

4.1. The Cox Proportional Hazards Model

The Cox proportional hazards model (PHM) is a relative risk model that describes the hazard rate of a component as a baseline hazard rate multiplied with its relative risk. This assumes that every component experiences the same base-level risk, depending on time, and its own relative risk, depending on its covariates. The model is given as

$$\begin{aligned}\lambda(t, \mathbf{x}_i) &= \lambda_0(t) \cdot r(\mathbf{x}_i), \\ r(\mathbf{x}_i) &= \exp(\mathbf{Z}_i' \boldsymbol{\beta}), \\ \mathbf{Z}_i &= f(\mathbf{x}_i),\end{aligned}\tag{4.1}$$

where $\lambda(t, \mathbf{x}_i(t))$ is the hazard rate at time t of component i , $\lambda_0(t)$ the baseline hazard rate and $r(\mathbf{x}_i)$ its relative risk. The latter term is composed of the derived covariates vector \mathbf{Z}_i associated with asset i and the coefficient vector $\boldsymbol{\beta}$. The derived covariates in \mathbf{Z}_i are obtained as functions of the basic data in \mathbf{x}_i .

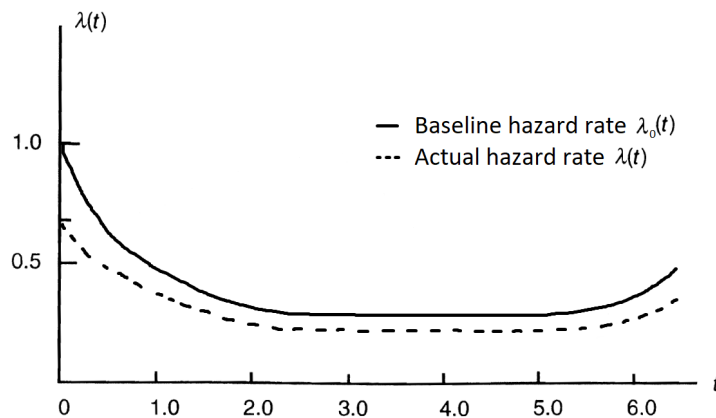


Figure 4.1: The baseline hazard $\lambda_0(t)$ and the actual hazard rate $\lambda(t, \mathbf{x}_i) = \lambda_0(t) \cdot r(\mathbf{x}_i)$. The relative risk $r(\mathbf{x}_i) \approx 0.7$.

An example of the typical ‘bath-tub curve’ baseline hazard rate $\lambda_0(t)$ and the multiplicative effect of the relative risk term $r(\mathbf{x}_i)$ is depicted in Figure 4.1. As can be seen, the baseline hazard rate is defined as a function over time. The actual hazard rate $\lambda(t, \mathbf{x}_i)$ is defined as a product of this baseline and the relative risk $r(\mathbf{x}_i)$.

To use this model, the baseline hazard function $\lambda_0(t)$ and the coefficient vector β need to be estimated. The estimates of the ‘true’ $\lambda_0(t)$ and β are denoted as $\hat{\lambda}_0(t)$ and $\hat{\beta}$ respectively. Furthermore, appropriate transformations $f(\cdot)$ of the basic data in \mathbf{x}_i should be selected to construct the derived covariates \mathbf{Z}_i , as most of the ‘raw’ data is not robust, and/or not log-linear in the hazard rate. These transformations are performed in chapter 3 and assessed in section 4.3.

4.1.1. Why This Model?

This model poses five main advantages over models discussed in section 1.2. First, the Cox PHM models the shared aging process of the components, while also accounting for individual factors. It does so in a flexible manner, making it simple to add new (IEC61850) data at a later stage, as discussed in the problem statement. Second, it is a robust model, as relatively few parameters need to be estimated and no distributional assumptions are required, in contrast with more traditional parametric models, such as the Weibull model, log-normal and log-logistic model [32]. This is convenient as the distribution is often complex, and few high quality data are currently available within TenneT TSO NL. Third, the baseline hazard function $\lambda_0(t)$ and the relative risk $r(\mathbf{x}_i)$ are independent of each other, meaning they can be estimated as such without risk of compounding error terms. Fourth, it accounts for time to failure and censoring, in contrast to e.g. logistic models. Last, it is a widely researched ‘workhorse’ model with a proven track record, making it appealing to industry.

4.1.2. Proportionality Assumption

The Cox PHM assumes proportionality between assets. This states that the hazard ratio, the ratio between the failure rates of two assets with at the same time t , is constant over time:

$$\frac{\lambda(t, \mathbf{x}_i)}{\lambda(t, \mathbf{x}_j)} = \frac{r(\mathbf{x}_i)}{r(\mathbf{x}_j)} = \frac{\exp(\mathbf{Z}'_i \beta)}{\exp(\mathbf{Z}'_j \beta)} = \exp((\mathbf{Z}_i - \mathbf{Z}_j)' \beta) \quad (4.2)$$

This assumption is assessed in section 4.3. For most of the covariates in the dataset, this can hold. However, with time-dependent covariates, such as the SF₆ leakage rate, this assumption is intrinsically violated. If the assumption does not hold, the extended Cox model is acquired, which is essentially the same model, but the hazard ratio only is defined for a certain time t . Research shows however, that slight deviations from this assumption do not invalidate results [33]. The leakage rate is treated as a constant covariate with constant hazard ratio as it is a random and likely slowly varying process over time and, due to insufficient data, it already needs to be assumed constant.

4.1.3. Time to Failure Interpretation

Two interpretations of time to failure are considered: major failure, signaled by replacement, and minor failure, signaled by corrective maintenance. The former is calculated by the time between the installation and the decommissioning of the asset. The latter is calculated as the mean time between corrective maintenance operations on the asset.

An example: a circuit breaker is installed in 1982, decommissioned in 2019 and receives 3 corrective maintenance operations. Using the age at replacement, the time to major failure of the asset is 2019 – 1982 = 37 years. Using the mean time between corrective maintenance operations, the time to minor failure is calculated as 2019 – 1998 = 21 years, divided by 3 failures, yielding a time to minor failure of 7 years. Here, it is accounted for that the register for minor failures dates back to 1998. This means that any minor failures before 1998 are not observed, making the data left-censored.

4.2. Model Estimation Method

In this section, the twofold estimation of the Cox PHM is treated. First, the coefficient vector β needs to be estimated. This estimation is executed through maximum partial likelihood with Newton-Raphson iterations, being the standard recommended method for this type of estimator. Second, the baseline hazard rate λ_0 is to be estimated, for which we apply the Kalbfleisch-Prentice estimator. The mechanics

behind this estimator are similar to the popular Kaplan-Meier estimator, but it accounts for the relative risk term $r(\mathbf{x}_i)$ [34].

4.2.1. Coefficient Vector β

The estimation of β is executed through maximizing its partial likelihood [13]. In this fashion, information on β that is entangled with information on the baseline failure rate can be extracted. This is convenient, as it allows for separate estimation of $\lambda_0(t)$ and β , and independence of estimation errors. In the next sections, we derive this estimator and discuss the handling of tied failure times.

Derivation of the partial likelihood estimator

In this section, [32] is closely followed for the derivation of $\hat{\beta}$. This is the partial likelihood estimator for the coefficient vector β , first introduced by [35].

Let the random failure time data T depend on probability density function $f(t; \lambda_0(\cdot), \beta)$. As β is to be estimated, we want to disentangle the relation between $\lambda_0(\cdot)$ and β . The partial likelihood is the means to that end.

Suppose now that a sample is drawn of T of size n , e.g. n circuit breakers in the population. Furthermore, suppose that of those n samples, only k are observed until failure within the window of the study; the remaining $n - k$ samples are right-censored. A failing asset is signified with j and failure time t_j . Let a_j indicate that asset j fails in the time interval $[t_j, t_j + dt_j)$ and b_j contain the information on censoring in $[t_{j-1}, t_j)$. Moreover, let $a^{(j)} = (a_1, \dots, a_j)$ and $b^{(j)} = (b_1, \dots, b_j)$. Now, we assume that the likelihood, depending on the sequence of $a^{(k)}$ and $b^{(k)}$, can then be written as

$$L(\lambda_0(\cdot), \beta) = \prod_{j=1}^k f(b_j | b^{(j-1)}, a^{(j-1)}; \lambda_0(\cdot), \beta) \prod_{j=1}^k f(a_j | b^{(j)}, a^{(j-1)}; \beta). \quad (4.3)$$

However, as we are only interested in β , we can omit the first term, as this term only contains information on the exact time of censoring. This way, we can base all inference on the second term, which describes observed asset failures. This is typical in cases where information on β in the first term is assumed to be irretrievably mixed up with information on $\lambda_0(\cdot)$. This second term only depends on β and is called the *partial likelihood*, as it is not a likelihood in the natural sense of the word and is conditioned on omitted terms.

The partial likelihood is then defined as

$$L(\beta) = \prod_{j=1}^k f(a_j | b^{(j)}, a^{(j-1)}; \beta), \quad (4.4)$$

which is the product of all the probabilities of failures, conditioned on all censoring and failure information leading up to event time t_j^- . We assume that the censoring mechanism is independent, meaning that it merely indicates that the failure time is after the censoring time. Using this assumption, the partial likelihood of Equation 4.4 can be rewritten to

$$L(\beta) = \prod_{j=1}^k \frac{\lambda(t_j; \mathbf{x}_j) dt_j}{\sum_{\ell \in R_j} \lambda(t_j; \mathbf{x}_\ell) dt_j}, \quad (4.5)$$

where R_j denotes the set of assets 'at risk' at time t_j^- , consisting of all items that have not failed or been censored yet. These assets are signified with ℓ and associated basic and derived covariate vectors \mathbf{x}_ℓ and \mathbf{Z}_ℓ respectively. As the baseline hazard terms in Equation 4.5 cancel, the expression can again be rewritten to

$$L(\beta) = \prod_{j=1}^k \frac{\exp[\mathbf{Z}_j(t_j)' \beta]}{\sum_{\ell \in R_j} \exp[\mathbf{Z}_\ell(t_j)' \beta]}, \quad (4.6)$$

showing that the partial likelihood indeed only depends on β , and not on $\lambda_0(\cdot)$. Maximization is typically performed with iterations of Newton-Raphson. [32] show the corresponding log-likelihood to be strictly concave, meaning that $\hat{\beta}$ is unique. Furthermore, they show the estimator to be consistent.

Handling ties in the dataset

When there are tied time-to-failure data points, the likelihood should be adjusted, as their ordering in Equation 4.6 is no longer trivial. Since the dating of the CBs is relatively granular, there are some ties which have to be considered. For this, we follow the advice of [16] and [36] by applying Efron's approximation [37] to the partial likelihood. The derivation of this estimator is more daunting, and the reader is referred to [32] for a concise treatment.

Applying Efron's approximation leads to the reformulation of Equation 4.6 to

$$L(\beta) = \prod_{j=1}^k \frac{\exp[\mathbf{s}_j(t_j)' \beta]}{\prod_{r=0}^{d_j-1} \left\{ \sum_{\ell \in R_j} \exp[\mathbf{Z}_\ell(t_j)' \beta] - r \bar{A}(\beta, t_j) \right\}}, \quad (4.7)$$

where d_j denotes the amount of items that fail at time t_j . Furthermore, $\mathbf{s}_j(t_j) = \sum_{i=1}^{d_j} \mathbf{Z}_{j_i}(t_j)$ is the sum of all derived covariate vectors of the assets failing at time t_j and where

$$\bar{A}(\beta, t_j) = d_j^{-1} \sum_{\ell \in D_j} \exp[\mathbf{Z}_\ell(t_j)' \beta]. \quad (4.8)$$

Above, D_j is the set of labels j belonging to assets that fail at time t_j . The application of this approximation introduces a slight bias and does not provide an exactly consistent estimator. In general however, it produces good estimates and should be favoured over its alternatives [36].

4.2.2. Baseline Hazard Rate λ_0

The baseline failure rate is modelled using the Kalbfleisch-Prentice estimator for the survival function [35]. This estimator is analogous to the widely used non-parametric Kaplan-Meier estimator, but accounts for covariates of the Cox model. The Nelson-Aalen estimator (also called the *Breslow estimator*) is more commonly used and is similar [38]. However, this estimator has the undesirable properties that the estimated hazard contribution can exceed 1 and the survival function estimate will never reach 0, even if the last occurring event is an uncensored failure. Furthermore, [39] show in their comparison between the Kalbfleisch-Prentice and the Nelson-Aalen estimators that the former typically yields less bias and smaller relative mean squared error.

Derivation of the Kalbfleisch-Prentice survival function estimator

In this section, [32] is followed for the derivation, but adapted for continuous time. Let $\lambda_0(t)$ be the baseline hazard rate. Then

$$\Lambda_0(t) = \int_0^t \lambda_0(u) du \quad (4.9)$$

is the cumulative baseline hazard. Following the derivation of section A.1, the baseline survivor function is then defined as

$$F_0(t) = P(T > t) = \exp \left[- \int_0^t \lambda_0(u) du \right]. \quad (4.10)$$

The covariates in \mathbf{x} are accounted for in the model through the derived covariate vector \mathbf{Z} , to diversify the assets and their associated hazard rates. This yields the 'complete' survivor function

$$F(t; \mathbf{x}) = P(T > t; \mathbf{x}) = \exp \left\{ - \int_0^t \lambda_0(u) \exp[\mathbf{Z}' \beta] du \right\}. \quad (4.11)$$

Now, consider observations with distinct times t_1, \dots, t_k and covariate vectors \mathbf{x}_ℓ , where the observations in set D_i failed at t_i in the interval $[t_i, t_{i+1})$. Consequently, the likelihood function is defined as

$$L = \prod_{i=0}^k \left\{ \prod_{\ell \in D_i} [F(t_i^-; \mathbf{x}_\ell) - F(t_i; \mathbf{x}_\ell)] \prod_{\ell \in R_i - D_i} F(t_i; \mathbf{x}_\ell) \right\}, \quad (4.12)$$

which is analogous to the Kaplan-Meier estimate, except it accounts for the covariates in \mathbf{x} . Clearly, estimating the baseline survivor function using this likelihood places the probability mass exactly at the

observed failure times t_1, \dots, t_k . This recreates the typical staircase effect of the Kaplan-Meier estimator, as

$$\Lambda_0(t) = \sum_{j=1}^k (1 - \alpha_j) \mathbf{1}(t_j \leq t), \quad (4.13)$$

where $(1 - \alpha_j)$ is the discrete hazard mass at t_j . Substitution of the latter two equations gives¹

$$L = \prod_{i=1}^k \left\{ \prod_{j \in D_i} (1 - \alpha_i^{\exp[Z'_j \beta]}) \prod_{\ell \in R_i - D_i} \alpha_i^{\exp[Z'_\ell \beta]} \right\}, \quad (4.14)$$

which can be maximized with respect to $\alpha_1, \dots, \alpha_k$, where β is taken as its maximum partial likelihood estimate $\hat{\beta}$. Differentiation of the log-likelihood, as demonstrated in section A.2, gives

$$\sum_{j \in D_i} \frac{\exp[Z'_j \hat{\beta}]}{1 - \alpha_i^{\exp[Z'_j \hat{\beta}]}} = \sum_{\ell \in R_i} \exp[Z'_\ell \hat{\beta}], \quad (4.15)$$

which produces the estimate for every α_i . This equation can be directly solved if there are not failure time ties in the dataset. Otherwise, an iterative solution is needed to acquire the maximum likelihood estimator. The estimated cumulative hazard function $\hat{\Lambda}_0(t)$ is obtained by substituting α_i for $\hat{\alpha}_i$ in Equation 4.13. The baseline survivor function and hazard rate estimate $\hat{F}_0(t)$ and $\hat{\lambda}_0(t)$ respectively are acquired by

$$\hat{F}_0(t) = \prod_{i|t_i \leq t} \hat{\alpha}_i \quad (4.16)$$

and

$$\hat{\lambda}_0(t) = \frac{d\hat{\Lambda}_0(t)}{dt}. \quad (4.17)$$

4.3. Proportionality Assessment

In this section, we investigate the proportionality assumption, as presented in subsection 4.1.2, for the variables. This assumption states that the ratio between the hazard rates of two circuit breakers at identical component-age t remains constant throughout their failure-cycle, as is expressed in Equation 4.2. The proportionality is assessed by visual inspection before coefficients are estimated, as graphs can show more information than a single quantitative estimate and the risk of spurious correlations is elevated, as we are working with a large data set.

Overall, we find that the replacement policy of CBs clouds the relation between major failures and covariates. For this reason, the assumption does not hold for most covariates, but does hold when modelling minor failures.

4.3.1. Visual Inspection

The visual proportionality inspection is performed with plots of transformed survivor functions. The result is a $\log(-\log(\hat{F}))$ vs $\log(t)$ plot, where \hat{F} is the estimated survivor function and t the time in years. If the times to failure are Weibull-distributed, which typically is a stylized fact of survival analysis, the plot yields a straight line. This can be shown, as the hazard function of the standard two-parameter Weibull distribution is equal to

$$\lambda(t) = \lambda\gamma(\lambda t)^{\gamma-1}, \quad (4.18)$$

with survivor function

$$F(t) = \exp[-(\lambda t)^\gamma]. \quad (4.19)$$

Taking the $\log(-\log(\cdot))$ transformation, we find

$$\log(-\log(F(t))) = \gamma(\log(t) + \log(\lambda)). \quad (4.20)$$

By using the empirical estimate of the survivor function, the plot provides an empirical check and can supply an estimate of the slope through γ and the intercept through $\gamma \log(\lambda)$.

¹In Equation 4.14, a small mistake in [32, p. 115] is corrected, where indices were swapped erroneously.

Stratification

We stratify the data points over the covariate of interest, to assess the influence of the covariate. For example, we divide the sample set in categories of operating voltages. Afterwards, the stratified data sets are regressed on the associated failure times, to make the plots. The strata are chosen such that they all contain a reasonable share of the original data set, as can be verified by comparing the criteria with the histograms of chapter 3.

The proportionality assumption holds, if the curves of the stratified sets are parallel to each other. The reason for this is the fact that hazards in the Cox PHM are multiplicative, meaning that after the $\log(-\log(\cdot))$ transformation, they become additive. Furthermore, the ordering of the parallel curves implies which stratified data set experiences the highest hazard and which the lowest.

An Example

An exemplary set of survivor curves and their transformed counterparts is provided in Figure 4.2. On the left, three survivor curves are depicted, where the green line shows the highest fraction ($\sim 85\%$) of survived circuit breakers after 20 years. The red line shows the lowest fraction ($\sim 72\%$). This implies that the set belonging to the green line is of higher quality.

The transformed curves on the right of Figure 4.2 show that their shapes and the ordering have changed. The transformed survivor curves are reasonably straight, retaining still a slight downward curve. This means that the survivor curves slope downwards slightly harder than a fitted Weibull distribution. Furthermore, the inversion of the ordering makes sense, as the negative sign in the transformation flips the ordering over the X-axis.

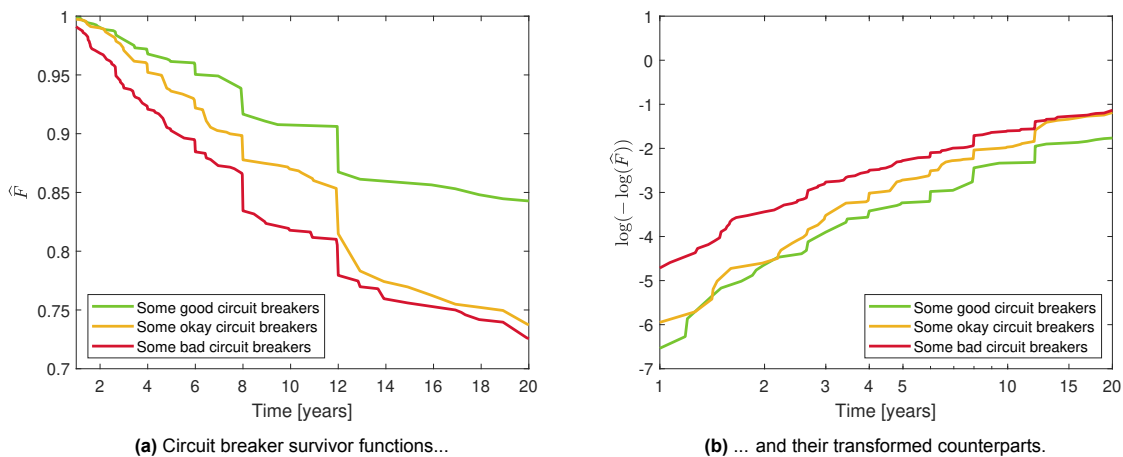


Figure 4.2: Example of the $\log(-\log(\hat{F}))$ vs $\log(t)$ transformation. Note the different X-axes' scaling.

Main Takeaway

When reading these plots, it is important to remember that the higher curves correspond to faster failing circuit breakers and vice versa. Furthermore, perfectly proportional hazards lead to curves perfectly parallel with a level shift. In practice, this property is not met completely, especially at the ends of the X-axis where extremem values reside. Nevertheless, reasonable inference can usually be made.

4.3.2. Time Since Last Failure

As we model both time to major and minor failure, they can serve as predictors for the other response variable. Ergo, time to minor failures can serve as a covariate to model the time to major failure and vice versa. In Figure 4.3, the time since last failure is stratified. On the left, the response variable is the time to major failure, and the regressor is the mean time between corrective maintenance. On the right side, the response variable is the time to minor failure and the regressor is the age of the component. The former is discarded, the latter is adopted into the model.

Major failure modelling

Figure 4.3 shows the strata of mean time between corrective maintenance not to intersect, but also not be completely parallel to each other. From a causal point of view, the ordering seems deceptive,

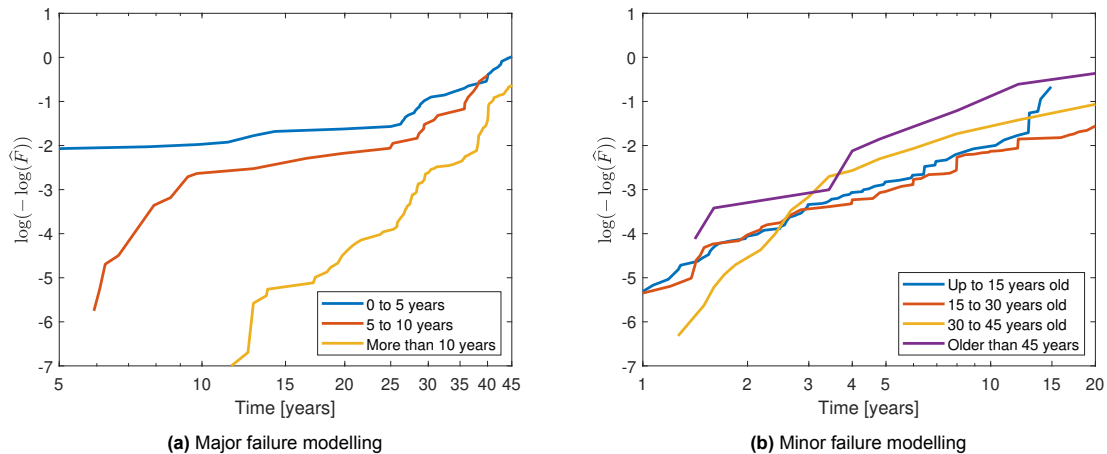


Figure 4.3: Stratification of the estimated transformed survivor functions across the (a) mean time between corrective maintenance and (b) component age.

as higher mean time between corrective maintenance is associated with higher survival probability. Intuitively, it would be expected that CBs that experience more minor failures should survive shorter. However, replacement is traditionally scheduled depending on age, not the amount of past failures. The reasoning therefore reverses: CBs that survive for longer are older and therefore exhibit more minor failures.

Following the above reasoning, this seems to be a bad regressor, as it appears to be an effect of a cause, the latter being the age at replacement. As implementation of this variable would merely model the current replacement policy, this should be omitted for actual health indexing and is therefore discarded.

Minor failure modelling

On the right side of Figure 4.3, the reverse case is shown, where the age is regressed upon the time to minor failure. As can be seen from the figure, there is some ambivalence between the strata. The curves seem relatively straight and parallel; only the yellow curve corresponding to CBs of ages between 30 and 45 years shows different behaviour for time to minor failure lower than five years. However, the lower (and higher) end of the X-axis mostly contains more extreme values, and irregularities here can be discarded if the middle section seems more unambiguous. For this reason, the component age seems to be reasonable regressor and is selected.

4.3.3. Manufacturer

As introduced in section 3.2, the 27 original manufacturers are reduced to 3 main manufacturers: Siemens, GE and Hitachi. Figure 4.4 shows them as three strata, with the two different response variables. For major failure modelling, the covariate is discarded, but it is selected for minor failure modelling.

Major failure modelling

The curves on the left side do not show a clear relation. Any relation between survivor probabilities and manufacturer seem to vary with age, or to be artefacts in the dataset. For this reason, the covariate is discarded.

Minor failure modelling

The frequency of minor failures seems to be more closely related with the manufacturer than the probability of major failures. As can be seen on the right side of the figure, CBs from Hitachi exhibit the lowest time to minor failure and CBs from GE the highest time to minor failure. This effect can be due to different quality standard of the manufacturers, or anything else related to their process.

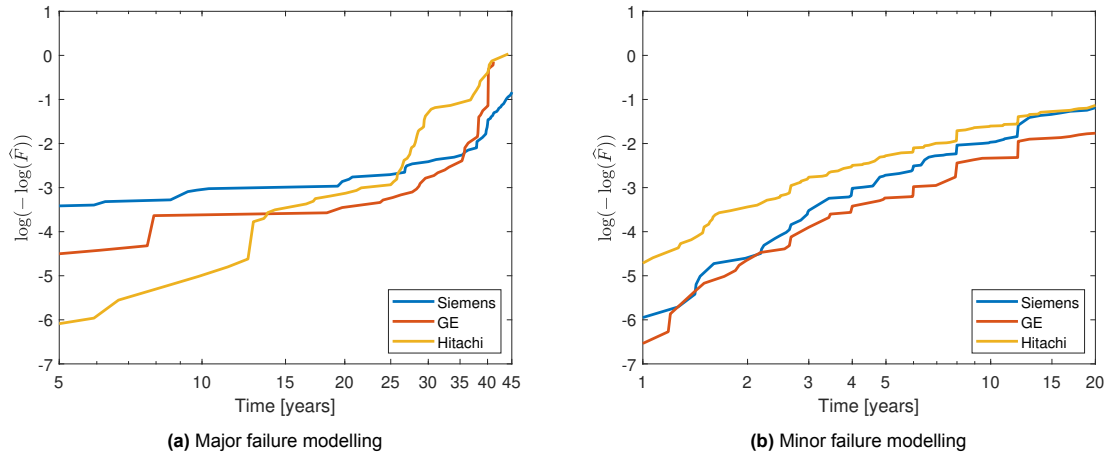


Figure 4.4: Stratification of the estimated transformed survivor functions across manufacturers.

4.3.4. Voltage Level

The four different voltage levels of the circuit breakers are stratified in Figure 4.5. It should be noted that the actual voltage present on the network levels may be different, as TenneT TSO NL can increase the voltage to increase transportation capacity. For this reason, direct relations between the voltage and the failure modelling should be disregarded, and only categorical inference can be made. For major failures, the covariate is discarded; for minor failures, it is not.

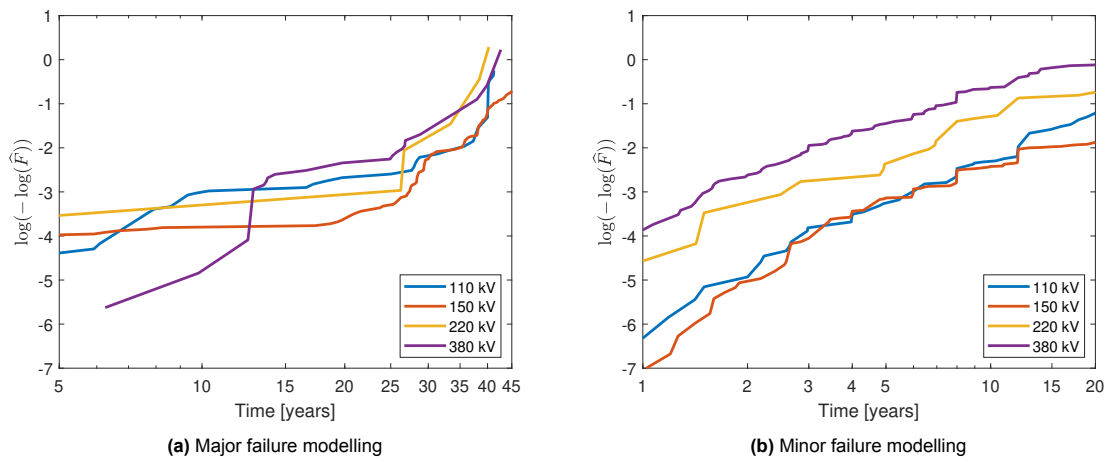


Figure 4.5: Stratification of the estimated transformed survivor functions across operating voltages.

Major failure modelling

The operating voltage seems to be somewhat related with the time to major failure, as higher voltage circuit breakers seem to be associated with the higher curves on the left side of Figure 4.5. However, the differences are minimal and not consistent across the board. Inference is hard, and the proportionality assumption likely does not hold. The covariate is discarded.

Minor failure modelling

On the right side, the voltage categories show a more clear relation with the time to minor failure. Higher voltage circuit breakers seem to require more corrective maintenance than lower voltage ones. Judging from the figure, the proportionality assumption seems reasonable.

Reasons for the increased hazard could be that higher voltage CBs typically transport more energy, meaning that switching involves more energy dissipation. This energy can increase wear of the arcing contacts or the decomposition of the SF_6 , which leads to impurities in the insulation medium.

Furthermore, higher voltage CBs often feature double arcing chambers, thereby increasing the leaking potential. The covariate is selected into the model.

4.3.5. Relative SF₆ Leakage Rate

The leakage rates are stratified across their average mass-percentage lost per year. The stratum with the highest values is open-ended, making it a catch-all for the extreme values in the distribution. The resulting curves are depicted in Figure 4.6. For major failures, this covariate is discarded, whereas for minor failures, it is selected.

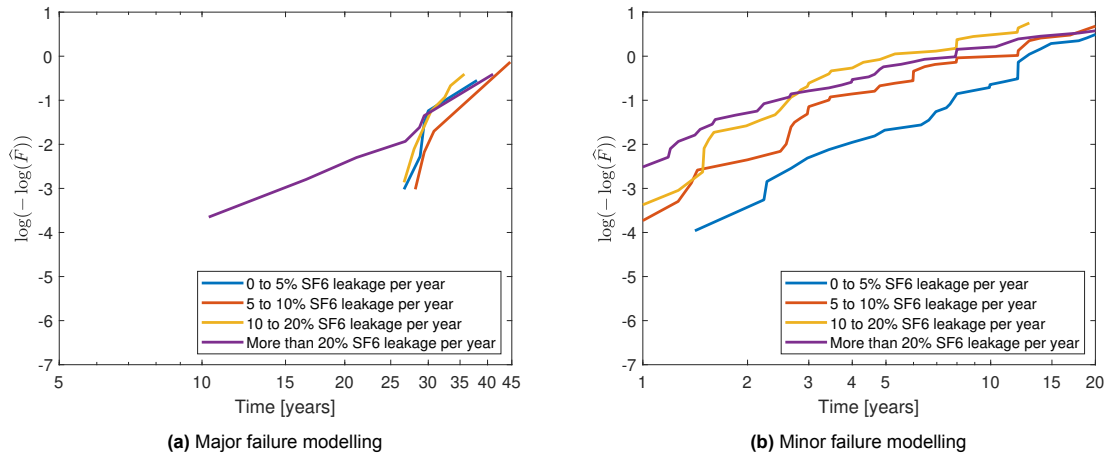


Figure 4.6: Stratification of the estimated transformed survivor functions across SF₆ leakage rates.

Major failure modelling

As can be seen on the left side of the figure, the curves are all relatively close together and intercept. Furthermore, the ordering is not increasing nor decreasing, indicating that the leakage rate does not contain information on the age at which the circuit breaker experiences major failure. Again, this is likely due to the policy of TenneT TSO NL, but is not reflective of the actual technical condition of the CB. The covariate is discarded.

Minor failure modelling

On the right side of the figure, it can be seen that a relation between the relative leakage rate and the time to minor failure seems plausible. The CBs that leak more than 20 %/y show a slightly lower hazard on the higher end of the time axis. This goes against the hypothesis of more leakage leading to more minor failures, but can be an effect of the relatively few circuit breakers with such drastic leakages.

Overall, the proportionality assumption seems reasonable, as well as the implied linear relation, since the distance between the 5 – 10 %/y and 10 – 20 %/y curves is approximately equal to the distance between the latter and the 10 – 20 %/y. This makes sense when considering the logarithmic transformation, as they both differ a factor two.

4.3.6. Switching Frequency

The registered average switching frequencies are stratified in four different ranges, as is shown in Figure 4.7. The stratum of more than 30 switching actions per year contains some extreme values, for which reason they are grouped together. For major failures, this covariate is discarded; for minor failures, it is selected.

Major failure modelling

As can be seen on the left side of the figure, the ordering of the curves is not consistent. The ordering during the first 25 years seems unreasonable as it is non-consecutive: with switching 10 – 20 times per year results in the highest hazard. This is followed by more than 30 times per year, then by 20 – 30, and last 10 – 20 times per year.

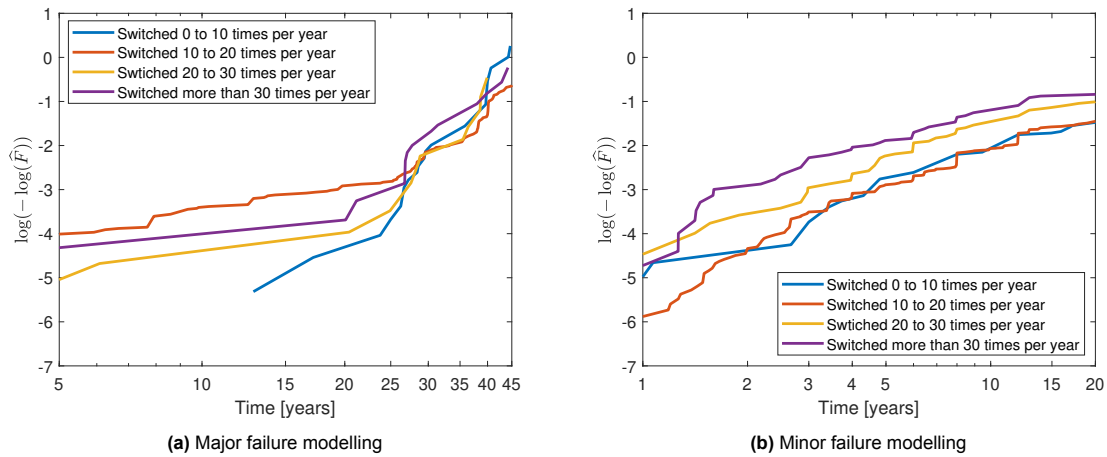


Figure 4.7: Stratification of the estimated transformed survivor functions across average switching frequencies.

This ordering seems to invert at the end of the CB life. This seems unnatural and defies the proportionality assumption. It is possible that a different amount of switching is beneficial during infancy and wear-out, but the results are not unambiguous enough to support such a hypothesis. For the mentioned reasons, this covariate is discarded for the modelling of major failures.

Minor failure modelling

On the right side of Figure 4.7, it can be seen that a relation such as discussed above is not present when modelling the time to minor failure. Here, the ordering of the strata falls in line with the initial hypothesis of more switching leading to more wear. The curves are reasonably straight and parallel, indicating that the proportional hazard assumption likely holds, though the first two levels of switching frequency seem to overlap somewhat.

It is possible that the latter indicates that occasional switching is beneficial to the technical state of the device to a certain degree. This would imply that CBs that very rarely switch experience issues associated with extended rest, such as rust and insufficient self-lubrication. Occasional switching could mitigate this, ensuring that the mechanics of the device remain in running-condition. Switching more often could cause excess wear, and again increased hazard. Furthermore, CBs with high switching frequencies are often associated with reactive loads, of which the currents are harder to switch. The covariate is selected for the model.

4.3.7. Periodic Maintenance Intensity

The intensity of periodic maintenance is split into three different strata, as can be seen in Figure 4.8. As there are some right-tail extreme values, these are gathered in a the stratum 'More than 0.2 times periodic maintenance per year'. For both failure definitions, the covariate is discarded.

Major failure modelling

As can be seen on the left side of Figure 4.8, no strong conclusions can be drawn from the stratification. There are some signs suggesting that increased periodic maintenance intensity results in higher hazard, but these are too disparate to be considered. The proportionality assumption likely does not hold. The covariate is discarded.

Minor failure modelling

In Figure 4.8b, it can be seen that the proportionality assumption is likely to hold for this changed response variable. It can be seen that an increase in periodic maintenance operations per year leads to increased hazard.

This does not fall in line with the hypothesis that periodic maintenance reduces the chance of future failures, by catching early signs of failure modes. However, it does not imply that periodic maintenance causes more failures, although this too is possible, as unnecessary maintenance poses the possibility for mistakes to be made by engineers.

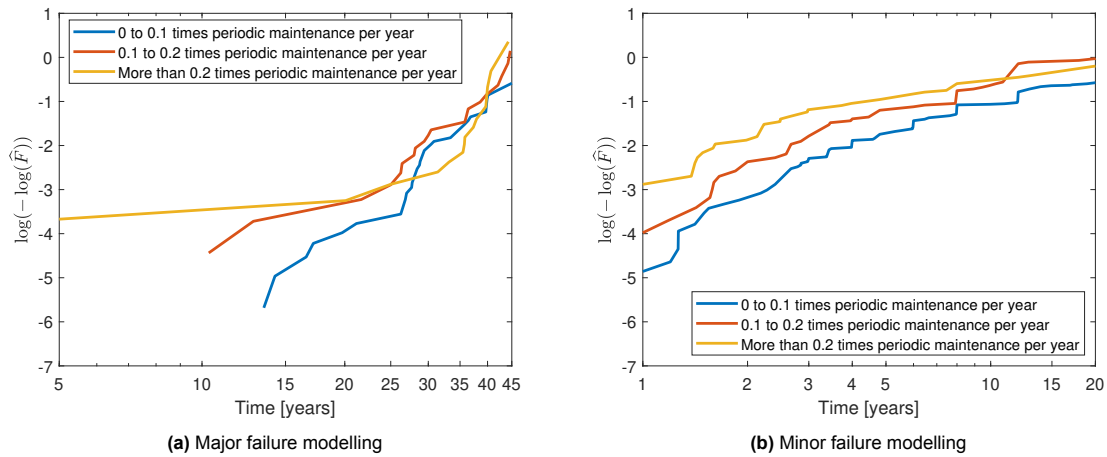


Figure 4.8

It could be that this is an artefact of the dataset, as a result of the maintenance policy. In TenneT TSO NL's current health index, the health of the component is lowered when it exhibits failures, leading to expedited periodic maintenance. This causes a correlation between the two, but with reversed causality.

We deem it unlikely that periodic maintenance really negatively affects the technical health of the component. Furthermore, as the goal of the new health index is to lower unnecessary periodic maintenance nevertheless, it seems unnecessary to introduce it into the model to further reduce periodic maintenance. This covariate is likely a result of the current maintenance policy, and should thus be treated as a response of the process, not as a regressor. The covariate is discarded.

4.3.8. Temperature

The year-averaged temperatures from the KNMI are stratified three-way. The results are depicted in Figure 4.9. For both failure types, the covariate is discarded.

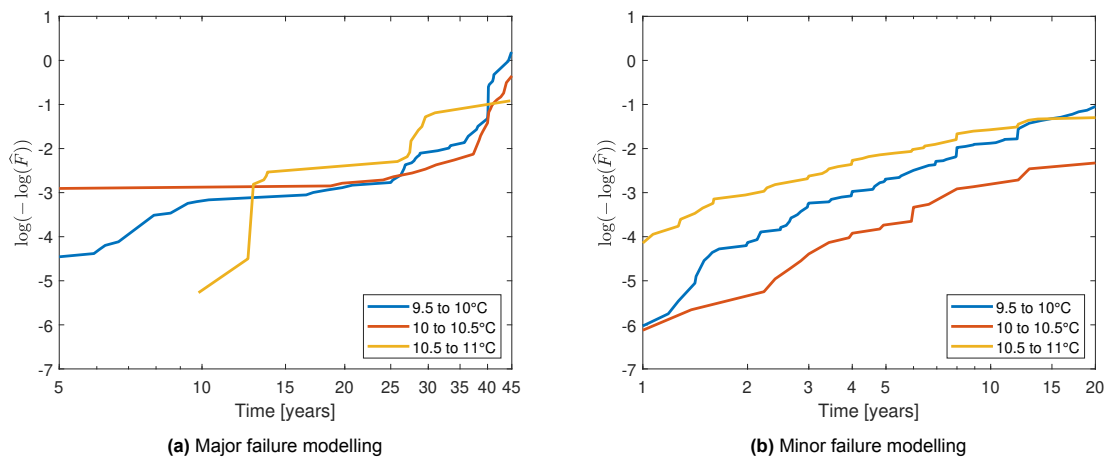


Figure 4.9

Major failure modelling

The resulting curves show many intersections and the ordering seems random. The proportionality assumption likely does not hold and the average temperature likely does not contain information on the remaining lifetime of the circuit breaker. The covariate is discarded.

Minor failure modelling

On the right side of the figure, the curves look straight and parallel, but the ordering is off. It seems very unlikely that a half degree Celsius difference causes such differences around an 'optimum' of 10 – 10.5 °C. For this reason, the covariate is discarded.

4.3.9. Relative Humidity

The year-averaged relative humidity from the KNMI measurements is stratified four-way. The results are depicted in Figure 4.10. Only for major failure modelling, the covariate is tentatively selected.

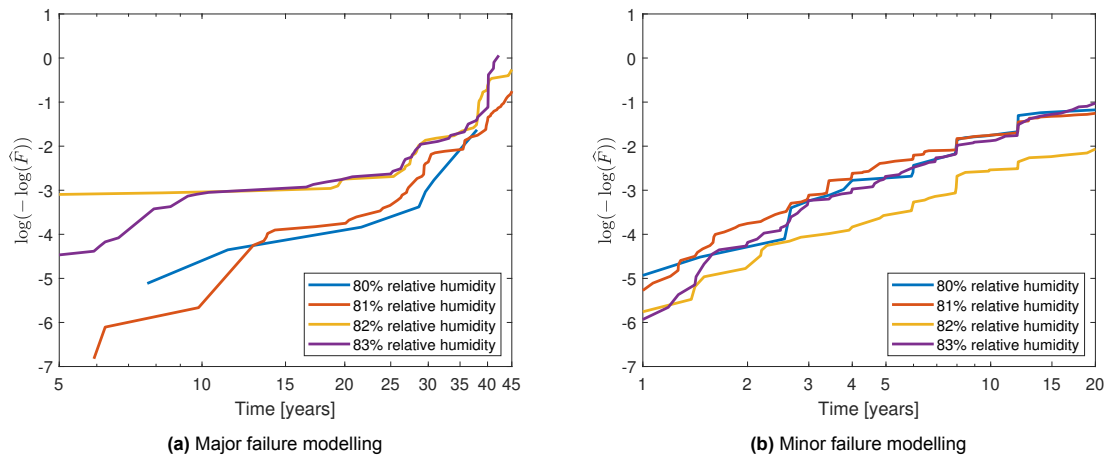


Figure 4.10

Major failure modelling

Interestingly, the relative humidity seems to form two strata: 80 – 81 % and 82 – 83 %. Even though these differences are small, the results seem to indicate a preference for lower humidity environments.

This could indicate that the higher humidity speeds up the rust process, increasing the hazard. This result should be taken with a grain of salt however, as the relative humidity differences of only a few percent are very small. Furthermore, the ordering in two groups remains unexplained. Still, the humidity is considered as a variable, as the proportionality assumption seems to hold.

Minor failure modelling

On the right side of the figure, it can be seen that no relation seems evident between the year-averaged relative humidity and the time to minor failure. The ordering is off and the curves intersect and overlap. The variable is discarded.

4.4. Regression Analysis

To assess the significance of the explanatory power of the covariates, a multiple regression is conducted. The goal of this is to finalize the model selection, and to estimate the coefficients thereof.

First, the correlation between the covariates is assessed with Kendall's τ , as it is the standard test for correlation on ordinal data. Afterwards, the methods introduced in section 4.2 are applied to the data to find coefficient estimates.

4.4.1. Correlation Assessment

As there are many covariates considered for the model, the table of estimated correlations is large. For this reason, the major results are discussed here and the complete table can be found in Appendix B.

Age – Mean Time Between Corrective Maintenance

The estimated correlation between 'Age' and 'Mean Time Between Corrective Maintenance' is 68.5%. This makes sense, as older components are more likely to worn out and fail.

Age – Periodic Maintenance Intensity

A correlation estimate is yielded of 20.3%. This seems reasonable, as very young components have not experienced periodic maintenance. Older components likely are scheduled for a check-up more often.

Manufacturer

The manufacturer dummy variables show a correlation estimate of -50.2%. This makes sense, as there are three different, almost uniformly distributed manufacturers being modelled by two dummies: if one of the dummies is equal to '1', the other is '0', yielding perfect prediction; if the former is '0', the other is a complete guess.

Voltage Level

The voltage dummies show a rank correlation estimate of -82.7%. The cause is the same as for the manufacturer dummies, except the distribution has changed. Most of the assets operate at either 110 or 150 kV and 220 kV is the reference voltage. Therefore, if the 380 kV dummy is '0', the 110/150 kV dummy is likely to be '1'.

Manufacturer – Voltage Level

The dummy variables for manufacturer and voltage show interactions, implying that one manufacturer is more likely to have been contracted for a certain voltage level than the other. From the correlation estimates, it can be deduced that GE is the dominant at the 110/150 kV level, Siemens at the 220 kV level and Hitachi at the 380 kV level.

SF₆ Leakage Rate – Periodic Maintenance Intensity

These covariates show a relationship of 21.2% rank correlation. This makes intuitive sense, as periodic maintenance can be intensified through TennaT's current HI when failures occur.

Temperature – Relative Humidity

Temperature and relative humidity are negatively correlated with an estimated Kendall's τ of -67.7%. This is due to the climate of The Netherlands, and the relation can be seen in Figure 3.6.

4.4.2. Coefficient Estimates

The coefficient estimates for the multiple regression analysis are shown in Tables 4.1 and 4.2. The significance of the variables is calculated using their limiting distribution, as given in the following section. For the sake of comparability of the estimates, all covariates are normalized before regressing.

Asymptotic distribution of the estimated coefficient

Asymptotically, the coefficient vector estimate $\hat{\beta}$ is χ_p^2 -distributed as:

$$\hat{\beta} \sim \chi_p^2(\beta, I(\beta)^{-1}), \quad (4.21)$$

where p is the number of covariates and the observed information $I(\beta)$ is calculated as

$$I(\beta) = -\frac{\partial^2 \log L}{\partial \beta \partial \beta'} = \sum_{j=1}^k \mathcal{V}(\beta, t_j). \quad (4.22)$$

In the above equation, \mathcal{V} is the covariance matrix of the covariates Z , given by

$$\mathcal{V}(\beta, t_j) = \sum_{\ell \in R_j} [Z_\ell - \mathcal{E}(\beta, t_j)]^{\otimes 2} p_\ell(\beta, t_j), \quad (4.23)$$

and $\mathcal{E}(\beta, t_j)$ its expectation given by

$$\mathcal{E}(\beta, t_j) = \sum_{\ell \in R_j} Z_\ell \cdot p_\ell(\beta, t_j), \quad (4.24)$$

both weighted to their relative risk by

$$p_\ell(\beta, t_j) = \frac{\exp[Z'_\ell \beta]}{\sum_{i \in R_j} \exp[Z'_i \beta]}, \quad \ell \in R_j. \quad (4.25)$$

Major failure analysis

As can be seen from Table 4.1, only one coefficient is considered for the model. The other coefficients have all been discarded during the proportionality assessment. The remaining coefficient yields a significant estimate at the 5%-level and is emboldened.

Table 4.1: Coefficient estimates of the multiple regression to assess covariate selection with time to major failure as response variable. Positive coefficient estimates indicate increased hazard per unit and vice versa. Estimates significant at the 5%-level are typeset in bold.

Covariate	Coefficient estimate (standard error)	<i>p</i> -value
Relative Humidity	0.321 (0.067)	<0.001

'Relative Humidity' shows significant results with an estimate of 0.321 and a *p*-value of less than 0.1%. This implies that higher average relative humidity decreases the life expectancy of the CB. However, this causality seems questionable, as it was deemed in the previous section. Although the relation seems strong, this could be an artefact in the dataset. Higher frequency data could reveal this relation to be different.

For the final composition of the PHM for modelling major failures, only one covariate remains. This tells us that, with the current data quality and replacement policy, there is very little predictive power for modelling the remaining lifetime of CBs.

Minor failure analysis

The coefficient estimates of the multiple regression for modelling minor failures are given in Table 4.2. This regression contains five covariates, with manufacturer and voltage split over four dummies in total. As can be seen from the table, all of the covariates, with the exception of one, yield significant estimates at the 5%-level and are emboldened.

Table 4.2: Coefficient estimates of the multiple regression to assess covariate selection with time to minor failure as response variable. Positive coefficient estimates indicate increased hazard per unit and vice versa. Estimates significant at the 5%-level are typeset in bold.

Covariate	Coefficient estimate (standard error)	<i>p</i> -value
Age	0.088 (0.052)	0.094
Manufacturer dummy - Hitachi	-0.093 (0.047)	0.050
Manufacturer dummy - GE	-0.127 (0.052)	0.014
Voltage Level dummy - 110/150 kV	-0.415 (0.063)	<0.001
Voltage Level dummy - 380 kV	0.148 (0.058)	0.010
Relative SF₆ Leakage Rate	0.191 (0.014)	<0.001
Switching Frequency	0.100 (0.036)	0.005

'Age' gives a positive coefficient estimate, showing that increasing major failure age is associated with lower time to minor failure. However, the *p*-value of 9.4% shows this not to be a significant result.

The manufacturer dummies show Siemens to be the producer of relatively the least reliable CBs. In a univariate setting, this seemed to be Hitachi, but the model writes this off to the increased hazard at which most Hitachi CBs operate: 380 kV.

GE still seems to produce the most reliable CBs, with the lowest manufacturer dummy estimates of -0.127 and a *p*-value of 1.4%. Furthermore, the voltage level of 110/150 kV at which most of their CBs operate also yields the lowest hazard, with a dummy estimate of -0.415 and significance of less than 0.1%.

The coefficient for the relative SF₆ leakage rate is strongly positive with a value of 0.191 and a *p*-value of less than 0.1%. This shows a pronounced positive relationship between the leakage rate and the experienced hazard.

Last, the average number of switching operations per year is also significantly positive with an estimate of 0.100 and a *p*-value of 0.5%. This implies that higher average switching action per year is associated with shorter time to minor failure.

4.5. Summary

Major failures are difficult to model using the available covariates, whereas minor failures are more suited for this purpose. The estimation of the proposed model shows that for the analysis of major failures, very little predictive power is available in the covariates. Only one covariate, 'Relative Humidity', yields significant results. For the analysis of minor failures, there is predictive power to be found. For this approach, four covariates produce significant results at the 5%-level: 'Manufacturer', 'Voltage Level', 'Relative SF₆ Leakage Rate' and 'Switching Frequency'.

5

Results

In this chapter, we present the results from the fitted model. These results include the estimated coefficient vector $\hat{\beta}$ and baseline hazard function $\hat{\lambda}_0(t)$, as well as the distribution of predicted failure probabilities. This prediction shows which components are expected to experience failure(s) in the near future. Furthermore, an out-of-sample prediction for failures in 2022 based on data up to and including 2021 is presented to assess the predictive power of the model. Last, a possible conversion of the predicted failure probabilities into a color-coded score to be used by TenNET TSO NL is introduced.

5.1. Estimated Model

In this section, we discuss the estimates of the complete model. First, the final coefficient estimates in $\hat{\beta}$ are presented, after which the estimated baseline hazard function $\hat{\lambda}_0(t)$ is shown.

5.1.1. Coefficient Vector β

After the covariate selection of the previous chapter, the maximum likelihood estimation is performed once more, to acquire their values without interference from removed covariates. Furthermore, likelihood-ratio tests are performed to statistically test the significance of the complete coefficient vector.

The likelihood-ratio test is selected as it has the highest power of the standard tests for nested models. To this end, the difference of the log-likelihoods of the selected model and the restricted model without coefficients ($\beta = 0$) is calculated. The distribution of the test statistic is χ_n^2 , with the degrees of freedom n equal to the difference in the number of parameters between the two models.

Major failure analysis

The estimate of the only remaining covariate ‘Relative Humidity’ has not changed from its estimate in the previous chapter, as can be seen in Table 5.1. This makes sense, as no co-regressor has been removed with respect to the previous estimation.

Table 5.1: Coefficient estimates of the multiple regression with the selected covariates and time to major failure as response variable. Positive coefficient estimates indicate increased hazard per unit and vice versa.

Covariate	Coefficient estimate (standard error)	p -value
Relative Humidity	0.321 (0.067)	<0.001

The likelihood-ratio test is performed to test the goodness of fit of the model against the restricted model with $\beta = 0$. The resulting statistic is equal to 22.616, which yields a p -value of less than 0.1%. Since this is less than the threshold of 5%, we reject the null hypothesis that the unrestricted model is not a better fitting model.

Minor failure analysis

The resulting coefficient estimates change only slightly when removing dismissed covariates. This effect is shown in Table 5.2 and makes sense, as the removed covariate ‘Age’, is not strongly correlated with any of the remaining covariates.

Table 5.2: Coefficient estimates of the multiple regression with the selected covariates and time to minor failure as response variable. Positive coefficient estimates indicate increased hazard per unit and vice versa.

Covariate	Coefficient estimate (standard error)	p -value
Manufacturer dummy - Hitachi	-0.096 (0.047)	0.043
Manufacturer dummy - GE	-0.122 (0.052)	0.019
Voltage Level dummy - 110/1 50 kV	-0.407 (0.062)	<0.001
Voltage Level dummy - 380 kV	0.150 (0.058)	0.009
Relative SF ₆ Leakage Rate	0.192 (0.014)	<0.001
Switching Frequency	0.099 (0.036)	0.005

The resulting value from the likelihood ratio test against the smaller model of $\beta = 0$ is 351.100, with an associated p -value of less than 0.1%. Once again, we reject the null hypothesis and accept the larger model as the better fit.

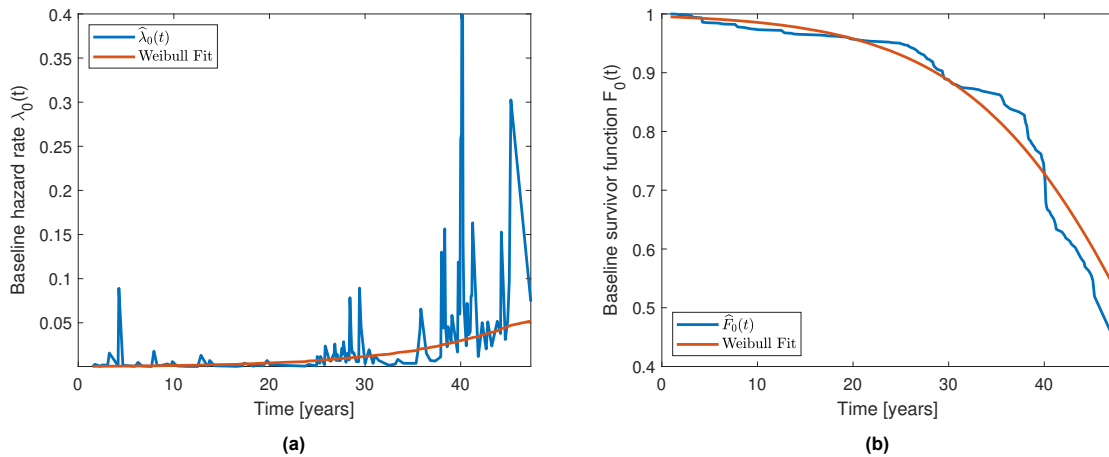
5.1.2. Baseline Hazard Rate λ_0

The estimated baseline hazard rate $\hat{\lambda}_0(t)$ and its associated survivor function $\hat{F}_0(t)$ for major failures are depicted in Figure 5.1. The respective estimates for minor failures can be seen in Figure 5.2.

As empirical estimates of both these functions are quite noisy, we have fit Weibull distributions upon them, to analyze trends and get a smoother estimate. As we saw in section 4.3, the Weibull fit seems reasonable for the considered data.

Major failure analysis

As can be seen in Figure 5.1(a), the empirically estimated hazard rate is relatively spiky, with the largest outliers at the standard decommissioning age of forty years. Furthermore, a small spike at infancy can be seen at approximately four years. This is typical for failure rates, showing slight confirmation of the bath-tub curve. The fitted Weibull curve captures the upward trend, showing increasing hazard with age.

**Figure 5.1:** Estimates of (a) the baseline hazard function $\lambda_0(t)$ and (b) the survivor function $F_0(t)$ and their associated Weibull fit for major failures.

Looking at the estimated survivor function in Figure 5.1(b), we see this effect more clearly. Most assets survive their younger years, but increasingly fail as they age. The Weibull fit can be seen to follow the curve neatly.

It should be noted that a significant part of the observations made here stem from TenneT's current decommissioning policy, which means many assets experience a truncated lifetime. However, if all components were run until actual major failure, a similar, but stretched curve would likely become visible. The reason for this is that CBs typically survive the designated forty years and failure would therefore happen at a later stage.

Minor failure analysis

Figure 5.2(b) shows a rather straight line for minor failures, in contrast with the estimated survivor function for major failures. Due to the granularity of mean time between corrective maintenance operations as work orders only date back to 1998, large steps can be observed at 24, 12 and 8 years, corresponding to components that experienced 1, 2 or 3 failures in the entire period of observation. However, the Weibull fit captures the straight trend.

Figure 5.2(a) therefore also shows a straight line for the baseline hazard rate estimate. This falls in line with expectation, as minor failures typically follow a more geometric-like distribution, with constant hazard rate. The spikes in the figure again correspond to the granularity of the data, but suggest a relatively constant $\lambda_0(t)$, even implying that a time-independent λ_0 might be more appropriate.

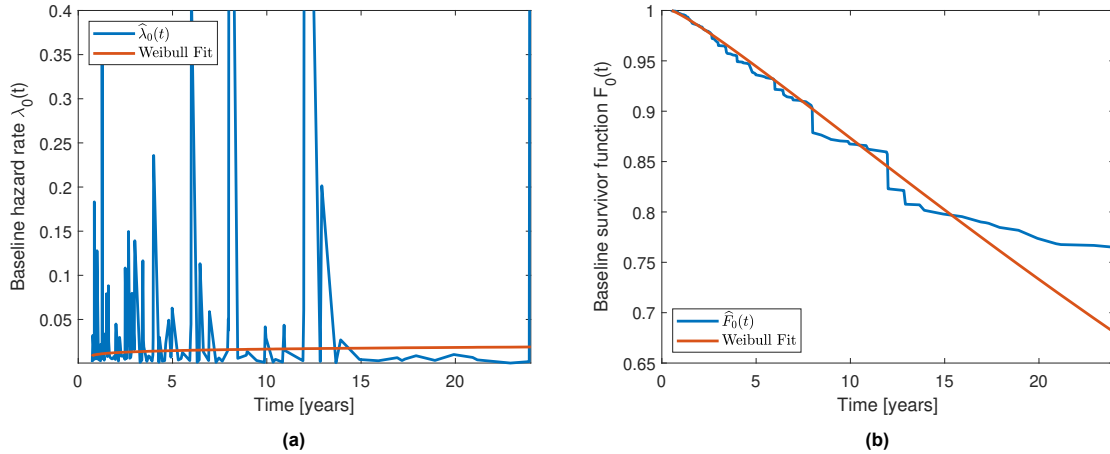


Figure 5.2: Estimates of (a) the baseline hazard function $\lambda_0(t)$ and (b) survivor function $F_0(t)$ and their Weibull fit for minor failures.

5.2. Distribution of Estimated Failure Probabilities

Using the estimated coefficients and baseline hazard, we can make a prediction of the hazard the assets will experience in the future. The experienced hazard is the cumulative hazard $\Lambda(t)$, equal to the integral of the hazard rate $\lambda(t)$. The probability of surviving a certain amount of hazard is given as:

$$F(t) = \exp(-\Lambda(t)), \quad (5.1)$$

as we derived in section A.1. Using this relation, the distribution of predicted cumulative hazard is transformed to estimated probabilities of failure over a certain horizon.

In Figure 5.3, the distribution of estimated failure probabilities for both major and minor failures is depicted. The horizon taken for this probability is one year, as this will be used in section 5.3, and is thus calculated as:

$$\hat{F}(t \leq T \leq t+1) = \hat{F}(T=t) - \hat{F}(T=t+1) = \exp(-\hat{\Lambda}(t)) - \exp(-\hat{\Lambda}(t+1)). \quad (5.2)$$

The estimated baseline hazards are approximated by using their Weibull fits, to smooth out the spikes.

Major failure analysis

As can be seen from Figure 5.3(a), all assets are estimated to have a very low probability of major failure in the upcoming year. This makes sense, as it is a relatively short horizon. If the horizon were to be increased, higher probabilities would become visible.

The shape of the distribution however suggests that most of the assets have a less than 1% chance of failing majorly in the coming year, whereas the more vulnerable components experience a probability of between 2% and 3%. This falls roughly in line with the findings of chapter 2, stating that major failures occur once every 200 circuit breaker years.

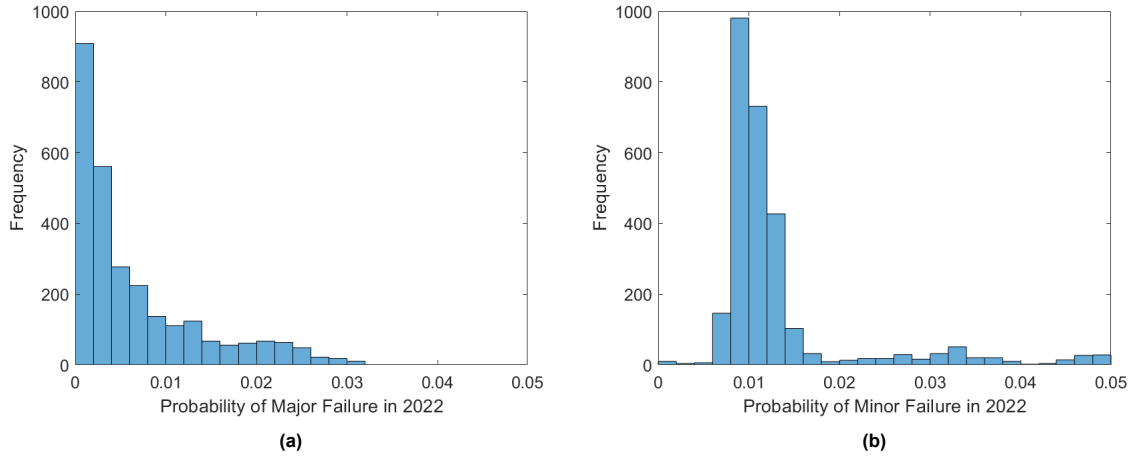


Figure 5.3: Histograms of predicted probabilities of (a) major failures and (b) minor failures in 2022.

Minor failure analysis

For the probabilities of minor failure, the shape of the distribution is different. Most assets experience a probability of approximately 1% to show a minor failure in the upcoming year. This falls in line with the approximately constant hazard rate, indicating that an asset is almost equally likely to fail at any age in the baseline case.

Vulnerable components have estimated probabilities of between 2% and 5%, where two humps are visible in the data, caused by the manufacturer dummy variables. Probabilities below 1%, suggesting high resiliency to failure, are scarce.

5.3. Assessment of Predictive Power

In this section, we assess the out-of-sample predictive power of the model. First, the failure probability distributions of failed and surviving components of 2022 are compared, both visually and statistically. Afterwards, the model is fit onto data up to and including 2021 and predicting which assets will fail in 2022. The coefficient estimates are very comparable to those of section 5.1 and are therefore given in Appendix C.

5.3.1. Bifurcation of Probability Distribution into Failed and Non-Failed

The distributions of estimated failure probabilities of Figure 5.3 are split into two categories: components that actually failed in 2022, and components that did not. The distributions are bifurcated and shown together in Figure 5.4.

As can be seen in the histograms, the frequency order of the failed and non-failed distributions differ, as well as their shape. The orange histogram contains the (few) failures, the blue histogram the (many) survivors. The difference in shapes confirms that the estimated failure probabilities are actually correlated with higher failure probability.

We apply the Monte Carlo permutation test to statistically assess this shape difference, as the sample size is too large for a full permutation test. This test is chosen as it is non-parametric and exact. The log-likelihood l of observing the failures with the predicted failure probabilities is given as:

$$l = \sum_{i=1}^n \log \left(p_i^{a_i} \cdot (1 - p_i)^{1-a_i} \right), \quad (5.3)$$

where, for asset i in the specified time-interval, p_i is the predicted failures probability and a_i is an indicator for actual failure. The null hypothesis states that the assignment of failures over the predicted probabilities is random and the blue and orange samples are therefore drawn from the same distribution.

Through Monte Carlo sampling, the failure labels a are randomly reassigned to predicted failure probabilities p 10.000 times and the corresponding log-likelihoods are calculated using Equation 5.3.

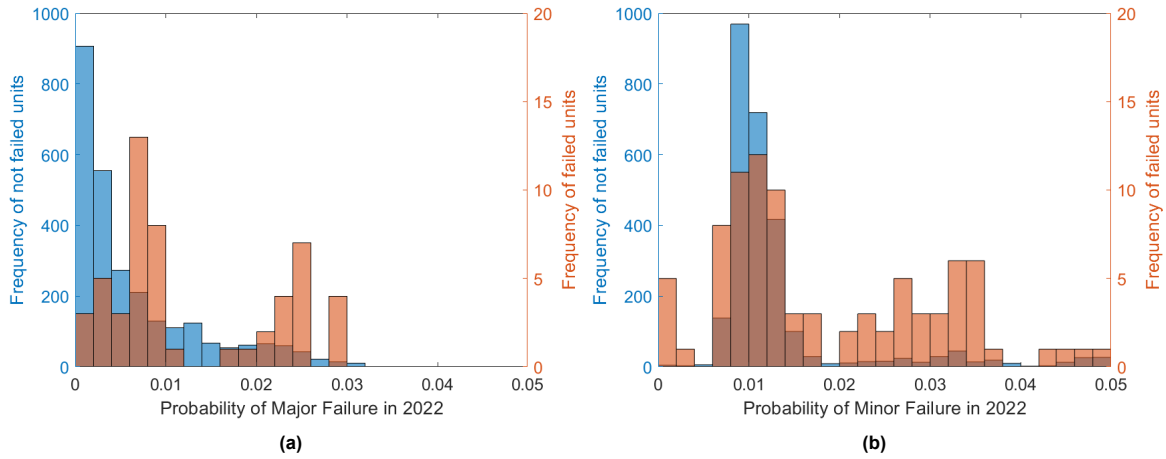


Figure 5.4: Bifurcated histograms of predicted probabilities of (a) major failures and (b) minor failures in 2022. Orange bars contain failed assets, blue contains non-failed assets.

This way, a reference distribution for l is generated. The p -value is acquired by taking the relative rank of the log-likelihood l in the generated distribution.

For both major and minor failures, this results in a rejection of the null hypothesis with corresponding p -values of less than 0.1%. thereby suggesting that the estimated probabilities contain valid information on the failure behaviour of the CBs.

5.3.2. Predictive Classification

In this section, we train a classifier on data up to and including 2021, and let it predict failures in 2022. This horizon of one year is chosen, as fitting the model on fewer data turned out to be challenging. The classifier is trained by optimizing the F-score in back-test and classifies based on an estimated probability threshold: if the estimated probability exceeds this, a ‘positive’ i.e. failure is predicted. The F-score is the harmonic mean of the precision (the number of true positives divided by all positives) and recall (the number of true positives divided by true positives and false negatives). Therefore, it equally represents both these metrics.

For major failures, the trained threshold is equal to 1.9% chance failure. For minor failures, this is equal to 2.2%. Of course, this is lower than 50%, which is the natural threshold, above which the expected value would be failure. However, as the horizon is relatively short and we are dealing with a large sample, the threshold is lower. No single component reaches a very high estimated failure probability, yet some still fail. The goal is to capture these.

		Prediction outcome					Prediction outcome		
		p	n	total			p	n	total
Actual value	p'	17	35	52	Actual value	p'	38	53	91
	n'	213	2492	2705		n'	262	2404	2666
total		230	2527		total		300	2457	

Figure 5.5: Confusion matrix results from predicting (a) major and (b) minor failures in 2022 out of sample.

The confusion matrices in Figure 5.5 contain the results of the predictions for both major and minor failures. The resulting F-score for major failures is equal to 12.0%, and 19.4% for minor failures, which is both low. As can be seen, the predicted number of failures are 230 and 300 respectively, whereas the actual number of failures is lower at 52 and 91 respectively. This means that our classifier overestimates the number of failures. Furthermore, the number of false negatives is higher than the number of true positives in both cases, which means that less than half of the actual failures are actually caught by the classifier.

The performance of predictive classification is bad. It should be noted that a horizon of one year is short, and extending this could increase the performance. Furthermore, predictions could be improved with increased data quality, as well as observation frequency. Nevertheless, in its current state, the prediction itself does not perform sufficiently well to use in this time frame.

This does not necessarily invalidate the results, as bad performance can be caused by other reasons. First, we are modelling failure probability, which is a latent variable. This means that we observe something else (failure) than what is modelled (likeliness to fail), which inherently introduces prediction problems. Second, binary classification is hard, especially on a dataset where only 2% to 3% actually fails. Last, the prediction horizon is very short. The model is developed for a time frame of several years, or decades. Trying to shorten this to a single year, makes it very complex to pinpoint which component will fail in only twelve months.

For the above reasons, the predicted failure probabilities are still applied to the health index, but the horizon is extended. Furthermore, binary classification is not considered for the estimation of the health of a component, nor its score.

5.4. Conversion to Color-Coded Score

The last step for constructing the health index is the conversion the failure probabilities into a scoring system. The traditional HI scoring system of TenneT TSO NL consists of 10 levels, with 4 colors. These are depicted in Table 5.3 with their definitions.

Table 5.3: Definition of the TenneT TSO NL health index scores.

Level	Color	Definition
1	Purple	Within 3 years, 80% chance that the component is irreparably damaged
2	Purple	Within 3 years, 50% chance that the component is irreparably damaged
3	Purple	Within 3 years, 20% chance that the component is irreparably damaged
4	Red	Within 7 years, 80% chance that the component is irreparably damaged
5	Red	Within 7 years, 50% chance that the component is irreparably damaged
6	Red	Within 7 years, 20% chance that the component is irreparably damaged
7	Orange	Older than 75% of the average age
8	Orange	Between 60% and 75% of the average age
9	Green	More than 5 years old and less than 60% of the average age
10	Green	Less than 5 years old

The definitions of the levels currently have little meaning, as the failure probabilities are not estimated, and can therefore not be categorized. Furthermore, levels 7 through 10 are defined based solely on the age of a component, where 1 through 6 are based on failure probabilities. This discrepancy introduces unexpected behaviour in the health index. Lastly, it has been shown in [40] that certain levels are skipped when the hazard rate is Weibull-distributed. This means that, before level four is reached, level three is reached, as both probabilities are exceeded. Using the current HI, an inconvenient ordering of the components would be made.

For the above reason, we introduce a new ordering, based on consecutive thresholds of failure probabilities. For the horizon of the failure probability, we choose 5 years, as this is the average of the 3 and 7 in the current system. The thresholds are chosen based on the distribution of the failure probabilities, and are given in Table 5.4.

Furthermore, the 10 levels are concatenated into 4 uniquely color-coded levels, as the goal of the HI is to visualize technical condition. Quantitative information remains available in the failure probability.

Lastly, the score is based on the estimated probability of minor failure, as this has shown to be more

Table 5.4: Newly introduced health index score thresholds

Level	Color	Definition
1	Purple	Within 5 years, 15% or higher chance of minor failure
2	Red	Within 5 years, 10% – 15% chance of minor failure
3	Orange	Within 5 years, 5% – 10% chance of minor failure
4	Green	Within 5 years, less than 5% chance of minor failure

predictable in the current state. This is proven by the higher F-score in the previous section, as well as more significant covariates in the model. As minor failures can be seen as precursors to major failure, the same conclusions for decommissioning decisions can be made using this more accurate metric.

The resulting distribution of HI scores is depicted in the pie chart in Figure 5.6. The lion's share of 58% of the population is assigned a green score, with the remaining 42% distributed over the worse scores. 27% is given an orange score, indicating a state of increased vulnerability. The red share makes up 7% and contains components of which the technical condition is worsened even further. The last share with the purple score contains the last 7% of the components with the worst condition. As the estimated failure probability of this bin contains no upper limit, this share can also contain components with imminent failures ahead.

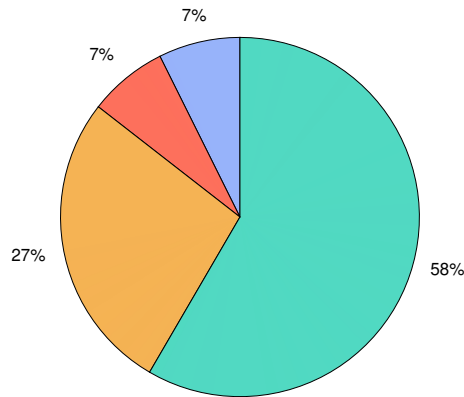


Figure 5.6: The scoring distribution of the components at the end of 2022, based on the failure probabilities output from the model and the definitions as given in Table 5.4.

As this scoring system is directly linked to the (quantitative) estimated failure probability, it is also possible to order the components according to their likeliness of failure. More than the scoring system, this could enable the operator to schedule maintenance first for the single highest risk-bearing component.

This system, with its fewer levels but more exact basis in statistics, should help TenneT TSO NL manage its assets more efficiently. Furthermore, its simpler definition should make using it for decision-making more intuitive for strategists and policy makers alike.

5.5. Summary

A four-level, color-coded scoring system for the technical health of the CBs has been formed using the results from the model. The distribution of predicted failure probabilities over a one-year horizon is analyzed, and bifurcated to assess the difference between failed and non-failed assets. It is concluded that significant predictive power is present, but binary prediction of asset failure in 2022 based on data up to and including 2021 does not yield satisfactory results. The prediction horizon is stretched to five years and the acquired predicted failure probabilities are converted into scores.

6

Conclusion

To unlock smarter and safer maintenance strategies for TenneT TSO NL's high-voltage assets, a data-driven health index is required to robustly assess the technical condition of the components. For this research, the problem is restricted to circuit breakers, as these are amongst their most complex assets.

In this report, a new health index for TenneT TSO NL's high-voltage assets is presented, meeting the outset goal. The conclusions are summarized through the answering of the research questions.

Main: How can the health of a live tank, spring-operated, high-voltage SF₆ circuit breaker installed onshore robustly be estimated using currently available monitoring data?

The health of the live tank, spring-operated high-voltage SF₆ circuit breaker can robustly be estimated using the new four-stage health index model, based on the Cox PHM. It allows for any type of input log-linear in the component's hazard rate to be used for modelling.

1. What is the distribution and rate of circuit breaker failure modes?

Failure modes are split into major and minor failure modes. Mechanical wear of the drive train and SF₆ leakages form the main contributors to circuit breaker failure. This is exhibited through the common major failure modes 'Does not open/close on command', related to mechanical failures, and 'Locked in open or close position', related to alarm signals from the control system. A common cause for the latter is the minor failure mode 'Small SF₆-leakage'.

Major failures are estimated to occur approximately once every 200 circuit breaker years, but the under-reporting of minor failures is too severe to make a reasonable estimate of its rate. Major failure rates roughly fall in line with the results of the failure probability modelling. Our modelling suggests that minor failures occur approximately twice as often.

2. What variables can be used for estimating the hazard rate of the circuit breaker?

Major failure data is relatively polluted, causing almost no information to be found in the covariates, with the exception of 'Relative Humidity'. The proportionality inspection and regressions show significant increasing hazard with increasing humidity, but a causal link is hard to define, as differences in average relative humidity are very small across the country.

Minor failure data is less censored and four significant covariates are found. GE is the manufacturer of the most reliable CBs, and Siemens those of the least. Furthermore, hazard rates increase with both the operating voltage and the average switching frequency. Last, the new estimate constructed for the SF₆ leakage rate significantly indicates increasing hazard associated with leakages. To the our knowledge, this is the first time that SF₆ leakage rates have been successfully used to model failure rates of circuit breakers.

3. How can the estimated hazard rate be translated into a health index scoring system?

The new HI scoring system is formed by categorizing the CBs based on their predicted probability of minor failure over a period of five years, as data on major failures are found to be too censored. The four colour-coded health index levels are chosen such that most healthy components with a reasonable failure probability get a good score, whereas components with increasingly higher failure probabilities get assigned increasingly worse scores.

6.1. Recommendations for Future Research

In addition to the conclusions presented above, three suggestions for future research are made below.

- A similar investigation on a more complete and longer data set might improve failure predictions, which currently perform below par. This could yield interesting predictive findings for policymakers and create a deeper understanding of the relation between the covariates and the failure behaviour.
- The incorporation of more climate change parameters, as will be introduced by IEC61850, can unlock detailed analysis of its effect of CB failures. Extreme weather conditions may have short-term effect on the technical condition of the asset, thereby rendering our approach with long-term averaged climate conditions ineffective.
- The analysis of the regressions residuals, could shed a more quantitative light on the log-linearity of the covariates in the hazard rates. This could be implemented by the well-known Cox-Snell residuals, martingale or Schoenfeld residuals, for different aspects of interest. Furthermore, a more strict approach to modelling the baseline hazard rate with e.g. the Weibull regression model requires more parameters, but would mitigate spiky hazard rates.

6.2. Recommendations for TenneT TSO NL

After conducting this research commissioned by TenneT TSO NL, three main recommendations for her *modus operandi* come to mind. These recommendations are listed below.

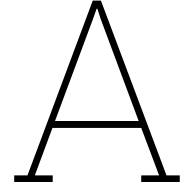
- The quality of the data available currently at TenneT TSO NL is too low to make accurate predictions. Furthermore, the organization thereof is such that it was relatively hard to find both the data themselves and colleagues who know how to find it. TenneT TSO NL should prioritize enabling her employees to construct it. Based on our findings, it should focus on switching frequencies and SF₆ leakage rates for CBs and extracting those in a digitized fashion.
- Switched current and motor current are likely to contain valuable information, based on the analysis of circuit breaker failures behaviour. This could also remove the endogeneity of the high-frequency switching of reactive loads, together with their higher switched current. As this data is currently not available, we were not able to investigate this quantitatively, but this is worth looking in to.
- The current health index levels are discrepant and said to be defined on failure probabilities, which are never actually estimated. TenneT TSO NL should construct a more coherent system, that is more intuitive to fill out and to use as a result. An example is provided in chapter 5, where we suggest new levels.

References

- [1] Siemens Energy, “Bringing zero closer: 3AV1 live tank circuit breaker,” 2022. [Online]. Available: <https://www.siemens-energy.com/global/en/offerings/power-transmission/portfolio/circuit-breakers/live-tank.html>.
- [2] R. D. Ross, *Reliability analysis for asset management of electric power grids*, 1st ed. Wiley, 2019, ISBN: 9781119125181.
- [3] CIGRE Working Group B3.48, “Asset health indices for equipment in existing substations,” CIGRE, Technical Brochure 858, Dec. 2021.
- [4] TenneT TSO, *Health index circuit breakers*, 2021.
- [5] B. Wells, K. Taylor, G. Howarth, *et al.*, “DNO common network asset indices methodology,” Ofgem, Apr. 2021. [Online]. Available: https://www.ofgem.gov.uk/sites/default/files/docs/2021/04/dno_common_network_asset_indices_methodology_v2.1_final_01-04-2021.pdf.
- [6] Cosmo Tech, *Master your asset investment strategies with digital twin simulation*, 2020. [Online]. Available: https://cosmotech.com/wp-content/uploads/2020/11/2-pager-Asset-Energy.pdf?utm_source=PDF&utm_medium=content&utm_campaign=Asset%5C%20Energy%5C%20Solution%5C%20Sheet.
- [7] D. Hughes, G. Dennis, J. Walker, and C. Williamson, “Condition based risk management (CBRM) - enabling asset condition information to be central to corporate decision making,” J. Mathew, J. Kennedy, L. Ma, A. Tan, and D. Anderson, Eds., Springer, 2006, pp. 1212–1217. DOI: 10.1007/978-1-84628-814-2_133.
- [8] A. N. Jahromi, R. Piercy, S. Cress, J. R. Service, and W. Fan, “An approach to power transformer asset management using health index,” *IEEE Electrical Insulation Magazine*, vol. 25, pp. 20–34, 2 2009. DOI: 10.1109/MEI.2009.4802595.
- [9] Meridium Inc., *Meridium AMP AHI*, 2016. [Online]. Available: https://www.ge.com/digital/documentation/meridium/V36100/PDF/Meridium_APM_AHI.pdf.
- [10] IBM, *IBM maximo asset performance management improves performance of business assets for reliability engineers and maintenance supervisors*, Oct. 2018. [Online]. Available: https://www.ibm.com/common/ssi/ShowDoc.wss?docURL=/common/ssi/rep_ca/9/872/ENUSAP18-0459/index.html&lang=en&request_locale=en.
- [11] M. S. Janssen, “Extending the scientific foundation of the DNV GL health index methodology for electrical power equipment,” Delft University of Technology, 2014. [Online]. Available: <http://repository.tudelft.nl/>.
- [12] W. Hu, P. Westerlund, P. Hilber, C. Chen, and Z. Yang, “A general model, estimation, and procedure for modeling recurrent failure process of high-voltage circuit breakers considering multivariate impacts,” *Reliability Engineering & System Safety*, vol. 220, p. 108 276, Apr. 2022. DOI: 10.1016/J.RESS.2021.108276.
- [13] D. R. Cox, “Regression models and life-tables,” *Journal of the Royal Statistical Society: Series B (Methodological)*, vol. 34, pp. 187–202, 2 Jan. 1972. DOI: 10.1111/J.2517-6161.1972.TB00899.X.
- [14] L. Brenière, L. Doyen, and C. Bérenguer, “Virtual age models with time-dependent covariates: A framework for simulation, parametric inference and quality of estimation,” *Reliability Engineering & System Safety*, vol. 203, p. 107 054, Nov. 2020. DOI: 10.1016/J.RESS.2020.107054.
- [15] P. Dehghanian, T. Popovic, and M. Kezunovic, “Circuit breaker operational health assessment via condition monitoring data,” *2014 North American Power Symposium, NAPS 2014*, Nov. 2014. DOI: 10.1109/NAPS.2014.6965427.

- [16] J. H. Jürgensen, "Individual failure rate modelling and exploratory failure data analysis for power system components," KTH Royal Institute of Technology, 2018, ISBN: 9789177299509.
- [17] E. J. de Haan, "High voltage asset performance modelling," Delft University of Technology, 2011.
- [18] TenneT TSO, *Company asset register*, 2021.
- [19] H. L. Resnikoff, "Mathematical aspects of reliability-centered maintenance," United Air Lines Inc., Tech. Rep., 1977.
- [20] CIGRE Working Group 13.06, "The first international enquiry on circuit-breaker failures and defects in service," *Electra*, vol. 79, pp. 21–91, Dec. 1981.
- [21] CIGRE Working Group 13.06, "Final report of the 2nd international enquiry on high voltage circuit-breaker failures and defects in service.," CIGRE, Technical Brochure 83, Jun. 1994.
- [22] CIGRE Working Group A3.06, "Final report of the 2004–2007 international enquiry on reliability of high voltage equipment, part 2 - reliability of high voltage circuit breakers," CIGRE, Technical Brochure 510, Oct. 2012.
- [23] A. Janssen, D. Makareinis, and C.-E. Sölver, "International surveys on circuit-breaker reliability data for substation and system studies," *IEEE Transactions on Power Delivery*, vol. 29, pp. 808–814, 2 2014, ISSN: 08858977. DOI: 10.1109/TPWRD.2013.2274750.
- [24] M. Runde, "Failure frequencies for high-voltage circuit breakers, disconnectors, earthing switches, instrument transformers, and gas-insulated switchgear," *IEEE Transactions on Power Delivery*, vol. 28, pp. 529–530, 1 2013. DOI: 10.1109/TPWRD.2012.2220638.
- [25] NERC Misoperation Information Data Analysis System, "MIDAS counts by region, cause and quarter 2017 - 2021," The North American Electric Reliability Corporation, 2021.
- [26] ENTSO-E Regional Group Nordic, "Grid disturbance and fault statistics," European Network of Transmission System Operators for Electricity, 2009.
- [27] IEC, "High-voltage switchgear and controlgear – part 1: Common specifications," International Electrotechnical Commission, IEC 62271-1, 2007.
- [28] A. Lathouwers, P. Jansen, and E. de Meulemeester, "Tennet's giant leap to be able to replace 140 substations within next 10 year, while in service and coming from different lay-outs," 2020.
- [29] M. van Eldik, "Circuit breakers: Determination of condition without physical inspection for circuit breakers," Hogeschool Saxion, Aug. 2020.
- [30] J. H. Jürgensen, L. Nordström, P. Hilber, A. L. Brodersson, and E. Andreasson, "Assessment of explanatory variables on the failure rate of circuit breakers using the proportional hazard model," in *2018 Power Systems Computation Conference*, IEEE, 2018, pp. 1–7. DOI: 10.23919/PSCC.2018.8442567.
- [31] Koninklijk Meteorologisch Instituut, *KNMI klimaatviewer*, 2020. [Online]. Available: <https://www.knmi.nl/klimaat-viewer/kaarten/>.
- [32] J. D. Kalbfleisch and R. L. Prentice, *The Statistical Analysis of Failure Time Data*, 2nd ed. Wiley, 2002. DOI: 10.1002/9781118032985.
- [33] M. J. Stensrud and M. A. Hernán, "Why test for proportional hazards?" *Journal of the American Medical Association*, vol. 323, pp. 1401–1402, 14 Apr. 2020. DOI: 10.1001/jama.2020.1267.
- [34] E. L. Kaplan and P. Meier, "Nonparametric estimation from incomplete observations," *Journal of the American Statistical Association*, vol. 53, p. 457, 282 Jun. 1958. DOI: 10.2307/2281868.
- [35] J. D. Kalbfleisch and R. L. Prentice, "Marginal likelihoods based on Cox's regression and life model," *Biometrika*, vol. 60, pp. 267–278, 2 Aug. 1973. DOI: 10.1093/BIOMET/60.2.267. [Online]. Available: <https://academic.oup.com/biomet/article/60/2/267/228987>.
- [36] I. Hertz-Picciotto and B. Rockhill, "Validity and efficiency of approximation methods for tied survival times in Cox regression," *Biometrics*, vol. 53, pp. 1151–1156, 3 1997. DOI: 10.2307/2533573.
- [37] B. Efron, "The efficiency of Cox's likelihood function for censored data," *Journal of the American Statistical Association*, vol. 72, pp. 557–565, 359 1977. DOI: 10.1080/01621459.1977.10480613.

-
- [38] W. Nelson, "Hazard plotting for incomplete failure data," *Journal of Quality Technology*, vol. 1, no. 1, pp. 27–52, 1969.
- [39] F. Xia, J. Ning, and X. Huang, "Empirical comparison of the breslow estimator and the kalbfleisch prentice estimator for survival functions," *Journal of Biometrics & Biostatistics*, vol. 9, pp. 1–7, 2 Oct. 2018. DOI: 10.4172/2155-6180.1000392.
- [40] S. Khuntia, "Substation use-case report using the asset tool from cosmo tech," TenneT TSO, Nov. 2021.



Derivations

This chapter contains derivations of properties used in the report. First is the relation between the survivor function $F(t)$ and the hazard rate $\lambda(t)$. Second is the derivation of the log-likelihood of the maximum likelihood estimator of α , required for the estimation of $\hat{\lambda}_0(t)$.

A.1. Derivation of Relation Between Survivor Function and Hazard Rate

Let T be a random variable representing the failure time. Then, the survivor function, failure probability and its probability density function are defined as

$$F(t) = P(T > t), \bar{F}(t) = P(T \leq t) \text{ and } f(t) = \frac{d}{dt} \bar{F}(t). \quad (\text{A.1})$$

The hazard rate $\lambda(t)$ and cumulative hazard $\Lambda(t)$ are defined as

$$\begin{aligned} \lambda(t) &= \lim_{\Delta t \rightarrow 0} \left(\frac{P(t < T \leq t + \Delta t \mid T > t)}{\Delta t} \right), \\ \Lambda(t) &= \int \lambda(t) \cdot d(t). \end{aligned} \quad (\text{A.2})$$

The hazard rate can be rewritten to

$$\begin{aligned} \lambda(t) &= \lim_{\Delta t \rightarrow 0} \left(\frac{P(t < T \leq t + \Delta t) \cap P(T \geq t)}{P(T \geq t) \cdot \Delta t} \right) \\ &= \lim_{\Delta t \rightarrow 0} \left(\frac{P(T \leq t + \Delta t) - P(T \leq t)}{F(T) \cdot \Delta t} \right) \\ &= \lim_{\Delta t \rightarrow 0} \left(\frac{\bar{F}(t + \Delta t) - \bar{F}(T)}{\Delta t} \right) \cdot \frac{1}{F(T)} \\ &= \frac{f(t)}{F(t)}. \end{aligned} \quad (\text{A.3})$$

This yields a relationship between the hazard rate $\lambda(t)$, the failure probability density function $f(t)$ and the survival function $F(t)$. Now, applying the derivative of a composite log function:

$$\frac{d}{dx} \ln(f(x)) = \frac{f'(x)}{f(x)}, \quad (\text{A.4})$$

the hazard rate can be expressed as

$$\begin{aligned}\lambda(t) &= \frac{d}{dt}(1 - F(t)) \cdot \frac{1}{F(t)} \\ &= -\frac{f(t)}{F(t)} \\ &= -\frac{d}{dt} \ln(F(t)),\end{aligned}\tag{A.5}$$

which is simply the negative derivative of the natural logarithm of the survival function. Integrating both sides of the equation yields the relation between the cumulative hazard and the survival function

$$\begin{aligned}\Lambda(t) &= -\ln(F(t)) \quad \text{and} \\ F(t) &= \exp(-\Lambda(t)).\end{aligned}\tag{A.6}$$

A.2. Derivation of the MLE of α_i

The likelihood function of Equation 4.14 is given as

$$L(\alpha) = \prod_{i=1}^k \left\{ \prod_{j \in D_i} \left(1 - \alpha_i^{\exp(\mathbf{Z}'_j \boldsymbol{\beta})}\right) \prod_{\ell \in R_i - D_i} \alpha_i^{\exp(\mathbf{Z}'_\ell \boldsymbol{\beta})} \right\}.\tag{A.7}$$

To derive the maximum likelihood estimate (MLE) α_i , we split the likelihood function over the non-censored distinct failure times k :

$$L(\alpha_i) = \prod_{j \in D_i} \left(1 - \alpha_i^{\exp(\mathbf{Z}'_j \boldsymbol{\beta})}\right) \prod_{\ell \in R_i - D_i} \alpha_i^{\exp(\mathbf{Z}'_\ell \boldsymbol{\beta})}.\tag{A.8}$$

Taking the logarithm of the likelihood function of α_i yields:

$$\ell(\alpha_i) = \sum_{j \in D_i} \log \left(1 - \alpha_i^{\exp(\mathbf{Z}'_j \boldsymbol{\beta})}\right) + \sum_{\ell \in R_i - D_i} \exp(\mathbf{Z}'_\ell \boldsymbol{\beta}) \log(\alpha_i),\tag{A.9}$$

of which the derivative with respect to α_i is

$$\frac{d\ell(\alpha_i)}{d\alpha_i} = \sum_{j \in D_i} \frac{0 - \exp(\mathbf{Z}'_j \boldsymbol{\beta}) \alpha_i^{\exp(\mathbf{Z}'_j \boldsymbol{\beta}) - 1}}{1 - \alpha_i^{\exp(\mathbf{Z}'_j \boldsymbol{\beta})}} + \sum_{\ell \in R_i - D_i} \frac{\exp(\mathbf{Z}'_\ell \boldsymbol{\beta})}{\alpha_i} = 0.\tag{A.10}$$

Above, the log-likelihood is equated to zero, to find the maximum likelihood solution for α_i . Multiplying both sides with α_i drops the right-hand side fraction:

$$\sum_{j \in D_i} \frac{\exp(\mathbf{Z}'_j \boldsymbol{\beta}) \alpha_i^{\exp(\mathbf{Z}'_j \boldsymbol{\beta})}}{1 - \alpha_i^{\exp(\mathbf{Z}'_j \boldsymbol{\beta})}} = \sum_{\ell \in R_i - D_i} \exp(\mathbf{Z}'_\ell \boldsymbol{\beta}).\tag{A.11}$$

Now, some juggling on the left-hand side will allow us to join the sets $R_i - D_i$ and D_i later on. This starts of as follows:

$$\sum_{j \in D_i} \frac{\exp(\mathbf{Z}'_j \boldsymbol{\beta}) \left(1 - \left(1 - \alpha_i^{\exp(\mathbf{Z}'_j \boldsymbol{\beta})}\right)\right)}{1 - \alpha_i^{\exp(\mathbf{Z}'_j \boldsymbol{\beta})}} = \sum_{\ell \in R_i - D_i} \exp(\mathbf{Z}'_\ell \boldsymbol{\beta}).\tag{A.12}$$

After this, the term on the left can be split into two terms:

$$\sum_{j \in D_i} \frac{\exp(\mathbf{Z}'_j \boldsymbol{\beta})}{1 - \alpha_i^{\exp(\mathbf{Z}'_j \boldsymbol{\beta})}} - \sum_{j \in D_i} \exp(\mathbf{Z}'_j \boldsymbol{\beta}) = \sum_{\ell \in R_i - D_i} \exp(\mathbf{Z}'_\ell \boldsymbol{\beta}),\tag{A.13}$$

the latter of which we can bring to the right side, while renaming the summation index j to ℓ :

$$\sum_{j \in D_i} \frac{\exp(\mathbf{Z}'_j \boldsymbol{\beta})}{1 - \alpha_i} = \sum_{\ell \in R_i - D_i} \exp(\mathbf{Z}'_\ell \boldsymbol{\beta}) + \sum_{\ell \in D_i} \exp(\mathbf{Z}'_\ell \boldsymbol{\beta}). \quad (\text{A.14})$$

Joining the summation sets, we find the maximum likelihood estimate by solving

$$\sum_{j \in D_i} \frac{\exp(\mathbf{Z}'_j \boldsymbol{\beta})}{1 - \alpha_i} = \sum_{\ell \in R_i} \exp(\mathbf{Z}'_\ell \boldsymbol{\beta}). \quad (\text{A.15})$$

If there are no ties in the dataset at time t_i , α_i is given by

$$\hat{\alpha}_i = \left\{ 1 - \frac{\exp(\mathbf{Z}'_i \hat{\boldsymbol{\beta}})}{\sum_{\ell \in R_i} \exp(\mathbf{Z}'_\ell \hat{\boldsymbol{\beta}})} \right\}^{\exp(-\mathbf{Z}'_i \hat{\boldsymbol{\beta}})}. \quad (\text{A.16})$$

If there are ties at t_i , a numerical solution to Equation A.15 is required. [32] suggest appropriate initial values for α_i .

B

Covariate Correlation Coefficients

This appendix contains the table for the estimated rank correlation coefficients between all of the covariates. These are estimated using Kendall's τ . As this table is symmetric, only the lower-left triangle is filled out. The results are depicted in Table B.1.

46

Coefficient	<i>see left-side</i>										
Age	1.000										
Mean Time Between Corrective Maintenance	0.685	1.000									
Manufacturer Hitachi	0.058	0.056	1.000								
Manufacturer GE	-0.018	0.027	-0.502	1.000							
110/150 kV	0.075	0.183	-0.232	0.264	1.000						
380 kV	-0.050	-0.159	0.248	-0.233	-0.827	1.000					
Relative SF ₆ Leakage Rate	0.053	-0.169	0.129	-0.028	-0.193	0.212	1.000				
Switching Frequency	-0.072	-0.100	-0.060	-0.034	-0.040	0.075	0.032	1.000			
Periodic Maintenance Intensity	0.203	-0.012	0.018	0.078	-0.077	0.108	0.318	-0.007	1.000		
Temperature	0.118	0.098	0.225	-0.092	0.072	0.062	-0.000	-0.004	-0.001	1.000	
Relative Humidity	-0.178	-0.129	-0.100	-0.010	-0.093	-0.040	-0.028	0.009	-0.079	-0.677	1.000

Table B.1: Kendall's τ correlation estimates between all the considered covariates

C

Out-of-Sample Model

In this appendix, the estimated model for the out-of-sample analysis of section 5.3 is presented. This model is fitted on data up to and including 2021, instead of up to and including 2022.

Table C.1 contains the estimates for the major failure model and Table C.2 for the minor failure model. Furthermore, Figure C.1 depict the estimated baseline hazard rate for (a) major failures and (b) minor failures, with their corresponding Weibull fits.

Table C.1: Coefficient estimates of the multiple regression with the selected covariates and time to major failure as response variable of data up to and including 2021. Positive coefficient estimates indicate increased hazard per unit and vice versa.

Covariate	Coefficient estimate (standard error)	<i>p</i> -value
Relative Humidity	0.351 (0.068)	<0.001

Table C.2: Coefficient estimates of the multiple regression with the selected covariates and time to minor failure as response variable of data up to and including 2021. Positive coefficient estimates indicate increased hazard per unit and vice versa.

Covariate	Coefficient estimate (standard error)	<i>p</i> -value
Manufacturer dummy - Hitachi	-0.099 (0.046)	0.031
Manufacturer dummy - GE	-0.119 (0.052)	0.022
Voltage Level dummy - 110/150 kV	-0.388 (0.062)	<0.001
Voltage Level dummy - 380 kV	0.161 (0.057)	0.005
Relative SF ₆ Leakage Rate	0.109 (0.027)	<0.001
Switching Frequency	0.087 (0.036)	0.015

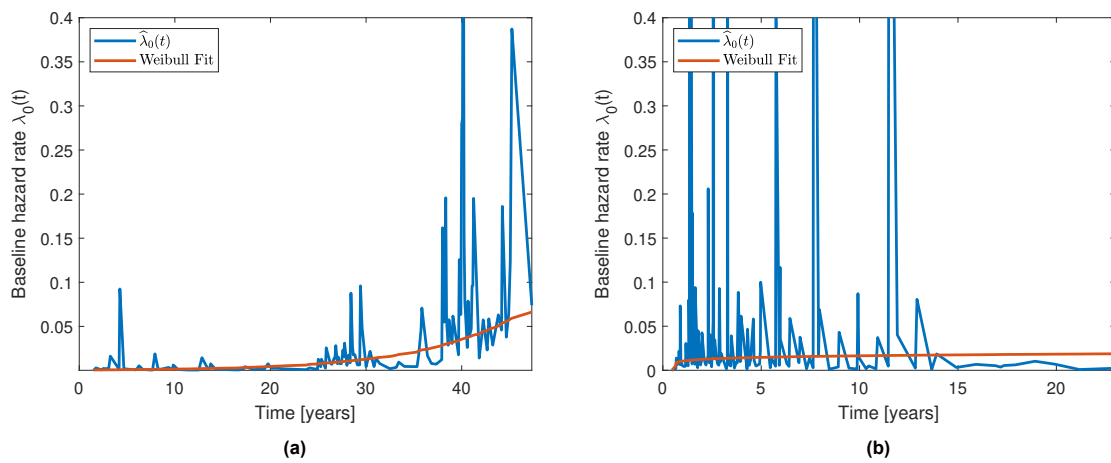


Figure C.1: Out-of-sample estimates of the baseline hazard function $\lambda_0(t)$ and their Weibull fits for (a) major and (b) minor failures.